

**Fakultät für Physik und Astronomie
Ruprecht-Karls-Universität Heidelberg**

Bachelorarbeit im Studiengang Physik
vorgelegt von

Sven Pirner

geboren in Gießen (Deutschland)

2010

Intelligent Filtering Algorithms for an upgraded Inner Tracker at ATLAS

Die Bachelorarbeit wurde von Sven Pirner ausgeführt am

Physikalischen Institut der Universität Heidelberg

unter Betreuung von

Herrn Prof. Dr. André Schöning

Zusammenfassung

Die Planungen für das Upgrade des Large Hadron Collider sehen vor die Design-Luminosität innerhalb des kommenden Jahrzehntes auf $10^{35} \text{ cm}^{-2}\text{s}^{-1}$ zu erhöhen. Allerdings bedeutet das auch, dass jedes interessante Kollisionsereignis von einer Vielzahl weiterer Ereignisse begleitet wird, welche das heutige Trigger Konzept des ATLAS Detektors herausfordern. Ein Ansatz die zusätzlichen Datenmengen schon im ersten Trigger-Level zu reduzieren besteht darin, die ihm zugänglichen Informationen um Spurdaten der Teilchen zu erweitern. Im Folgenden soll die Möglichkeit diskutiert werden, die Doppel-Lagen-Struktur der SCT-Detektoren zu nutzen, um den Transversalimpuls der Teilchen zu klassifizieren. Zusätzlich wird geprüft, in wie weit diese Doppellagenstruktur dafür verwendet werden kann, Interaktionen zwischen Teilchen und Detektor zu rekonstruieren, die aufgrund von einzelnen Ineffizienzen des Detektors verloren gegangen sind. Es wird gezeigt, dass es unter Ausnutzung von Informationen über die Anzahl der Detektorstreifen, die ein Teilchen beim Durchgang durch eine einzelne Detektorlage auslöst, möglich ist, diese Ziele zu erreichen.

Abstract

The planning for the LHC Upgrade foresees to increase the design-luminosity by an order of magnitude to $10^{35} \text{ cm}^{-2}\text{s}^{-1}$ within the next decade. Therefore all interesting events will be accompanied by several other events, which will challenge the recent trigger system of the ATLAS detector. One approach to reduce the additional amount of information in the first trigger level, is to add track information to its decision. In the following the possibility to exploit the double layer structure of the SCT-detectors in order to quantify the transverse momenta of the particles will be studied. Additionally it will be discussed how the double-layer-structure can be utilised to reconstruct interactions between particles and detector, which have gone lost due to single-hit-inefficiencies of the detector-strips. It will be shown that those objectives can be achieved by using information about the number of strips a particle passes by traversing a single detector layer.

Contents

Motivation	1
1. Introduction	3
1.1. The Large Hadron Collider	3
1.1.1. Accelerating Protons	3
1.1.2. Main Objectives of the Large Hadron Collider	3
1.1.3. The Large Hadron Collider Upgrade (SLHC)	5
1.2. The ATLAS Experiment	6
1.2.1. Basic Design of ATLAS	7
1.3. The ATLAS High Luminosity Upgrade	13
1.3.1. Inner Detector	13
1.3.2. ID Design Planning	13
1.3.3. L1 Trigger System	15
2. Monte Carlo Software	19
2.1. Idealised Detector Architecture	19
2.2. Framework of Simulations	19
2.2.1. p_T Distribution	20
3. Geometry	23
3.1. Trajectory in the Transverse Plane	23
3.2. Offset in z -Direction	27
4. Combined Algorithm	29
4.1. Selection of High Transverse Momentum Candidates	29
4.1.1. Reduction of Data Volume	30
4.1.2. Efficiency	32
4.2. Reconstruction of Lost Hits	32
4.3. Combined Algorithm	34
4.3.1. Efficiency	34
4.3.2. Reduction of Data Volume	36
5. Cluster-Size-Method	37
5.1. Cluster-Size	38
5.1.1. Filter Potential with respect to Silicon Thickness	38
5.1.2. Reduction of Data Volume	40

Contents

5.1.3. Decrease of the Maximum Search Offset	41
5.2. Efficiency Gain of the Combined Algorithm	41
6. Grouping Algorithm	45
6.1. Problem of the Combined Algorithm	45
6.2. Problem Solving	46
6.3. Implementation of Grouping	47
6.4. Efficiency	47
6.5. Reduction of Data Volume	50
7. Conclusion	51
7.1. Algorithm Efficiency	51
7.2. Reduction of Data Volume	51
A. Definitions and Illustrations	55
A.1. Hit	55
A.2. Coincidence and Offset	55
A.3. Hypothetical Coincidences	55
A.4. Lost Hits	55
A.5. Maximum Search Offset	57
A.6. Reduction of Data	58
A.7. Algorithm Efficiency	58
A.8. Detector Efficiency	58
A.9. Illustrations of Simulated Hit Pattern	58

Motivation

In September 2008 the world's largest experiment for particle physics - the *Large Hadron Collider* (LHC, cf. section 1.1) - was put into operation, in order to search for yet undiscovered particles, substructures of known particles as well as extra dimensions and with them evidence for new physics.

In addition to the collider experiments are also needed to capture and store the information generated by the collisions of hadrons. One of those six detector experiments is ATLAS (A Toroidal LHC Apparatus) which is described in section 1.2.

Even though the ATLAS detector experiment has started to collect data only recently, there are already plans for upgrading the Large Hadron Collider to collect more statistics by increasing its design luminosity¹ by an order of magnitude (cf. section 1.1.3).

Since such an increment will lead to more pile-up events² and hence to a huge increase in tracks per bunch crossing, this upgrade will challenge the current design of the ATLAS detector (cf. figure 1.3) from the perspective of detector performance and radiation tolerance. Especially its inner detector as well as its trigger system (cf. section 1.2.1) have to be adjusted to exploit all of the additional information being obtained by the LHC upgrade.

A certain move for the inner detector of ATLAS to maintain those challenges will be the increase of granularity, which has obvious advantages such as a lower detector occupancy and more detailed track information. On the other hand this accession of granularity leads to a greater amount of detector modules, which have to be read out in a give time. The latest studies of the planned ATLAS upgrade predict the number of channels in the inner detector to be in the order 300 million. Since the current trigger-system (cf. 1.2.1) is only capable of reducing the actual amount of data, other ways of reducing the bandwidth in a first trigger step have to be investigated.

The present thesis explores the possibility to exploit the double layer structure of the silicon micro-strip layers (SCT, cf. 1.2.1) to filter particles with a low transverse momentum p_T , which will be an essential step towards reducing the amount of information in the first trigger level (L1). This *self-seeded* approach only needs track

¹Meant is the instantaneous **luminosity** $L = fn \frac{N_1 N_2}{A}$ where f is the revolution frequency, n the number of bunches per beam, N_i number of particles in each bunch and A the cross section of the beam. There is also the integrated luminosity $\int L dt$, which will be used as a measurement for the amount of collected data.

²Simultaneous collisions, which are taking place in the same bunch crossing, are called **pile-up events**.

Motivation

information to decide whether or not a special region of the detector barrel contains a particle with a high transverse momentum.

In a second step the double layer structure will be utilised to reconstruct missing hits in one of the double layer in order to retain a high track-finding-efficiency for high momentum tracks.

Two algorithm generations are presented, which not only enable a trigger decision but also reconstruct lost hits based on a given hit pattern on a double layer detector. The first generation (cf. chapter 4) describes the basic idea behind the reconstruction of lost hits as well as the concept of data reduction. The large amount of particles with a low transverse momentum lead to suboptimal results for data reduction and for the recovery of lost interactions. Additional reasons for those results are the expected occupancy of approximately 2 % and the expected detector inefficiency.

Hence another idea is presented, which should reduce the number of particles with a very low transverse momentum: the cluster-size-method (cf. section 5).

The second algorithm generation (cf. chapter 6) is based on the cluster-size-method. It exploits the lack of particles with a very low transverse momentum to form isolated groups of hits. Due to the small number of hits per group the hit-association becomes less difficult. Therefore the identification and recovery of single-hit-inefficiencies can be improved.

1. Introduction

In the following a short overview about the LHC, the ATLAS detector and the upgrade planing for both is given. Since the present thesis concerns the inner detector as well as the trigger-system of the ATLAS experiment, those components are described in more detail.

1.1. The Large Hadron Collider

The Large Hadron Collider near Geneva, Switzerland is the last element of the accelerator complex hosted by the European Organisation of Nuclear Research (CERN) shown in figure 1.1. This synchrotron and storage ring is designed for colliding counter circulating bunches of protons with a total centre of mass energy up to $\sqrt{s} = 14$ TeV at the design luminosity of $10^{34} \text{ cm}^{-2}\text{s}^{-1}$ [1]. It will also collide heavy ions, in particular lead nuclei, at a centre of mass energy of 5.5 TeV and a design luminosity of $10^{27} \text{ cm}^{-2}\text{s}^{-1}$ [1].

1.1.1. Accelerating Protons

In a first step, protons - as a result of stripping orbiting electrons from a hydrogen atom - are accelerated to an energy of 50 MeV by Linac2 and injected into the PS Booster, where the protons are boosted at an energy of 1.4 GeV. After being yielded to the Proton Synchrotron and the Super Proton Synchrotron, the proton beams have an energy of approximately 450 GeV. Finally the proton beams enter the LHC in both - clockwise and anticlockwise - directions, where they can be accelerated to the maximum energy of 7 TeV each.

1.1.2. Main Objectives of the Large Hadron Collider

At a total centre of mass energy of 14 TeV per proton-proton pair it is possible to obtain a higher mass reach than ever before.

The most important advantage of those collision energies is the chance to study physics of the terascale and with it theoretical predictions not only for unobserved particles such as the Higgs boson (cf. 1.1.2) or supersymmetric particles (cf. 1.1.2) for instance, but also of additional dimensions..

1. Introduction

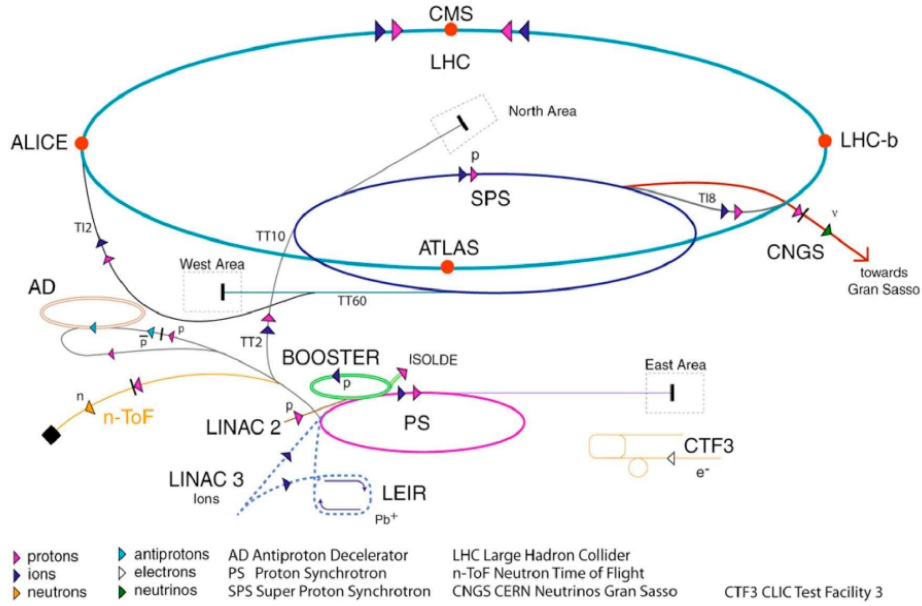


Figure 1.1.: The CERN accelerator complex in Geneva, Switzerland [2].

The Higgs Mechanism

One important task of the LHC and its detector devices is to provide evidences of the existence of the Higgs boson, an elementary particle postulated by R. Brout and F. Englert[3] as well as Peter Higgs[4]. The Higgs mechanism gives an explanation for how the masses of the W and Z bosons rise due to spontaneous electroweak symmetry breaking.

One fundamental aspect of this theory is to connect the mass of particles with the so called Higgs field, which - in theory - fills the whole space. Therefore verifying those postulates would help to understand the existence of massive particles.

Experiments made at lower centre of mass energies at the Large Electron Positron Collider (LEP - $\sqrt{s} = 209 \text{ GeV}$) and the Tevatron experiments ($\sqrt{s} = 1 \text{ TeV}$) in combination with statistical considerations lead to the conclusion that the mass of the lightest Higgs boson must be located between 114 GeV and 160 GeV [2]. Therefore if the Higgs field does exist, the associated Higgs boson should be detected by experiments at LHC.

The Theory of Supersymmetry

The other forecited important objective is verifying or neglecting the theory of supersymmetry by searching for the lightest supersymmetric particles.

The theory of supersymmetry postulates a so called *super-partner* for every standard-model particle. Those super-partners would be equal to the standard particles in every quantum state except for its spin which would differ by $\frac{1}{2}$. Since no supersymmetric particles have been found yet this symmetry must be broken and therefore allow the super-partners to be heavier than the standard-model particles.

Finding evidence for the existence of those particles would be a great advancement in particle physics, since the theory of supersymmetry allows a high-energy unification of strong interaction, weak interaction and the electromagnetism as well as providing a candidate for dark matter, which accounts for 23 % of the matter of the universe, where *ordinary* matter only accounts for 4.6 %.

Previous experiments at the Tevatron determined a lower mass limit for super symmetric particles of between 300 and 400 GeV [5].

Since there is no theoretical upper border for their mass, supersymmetric particles can be still too heavy to be produced at the LHC.

1.1.3. The Large Hadron Collider Upgrade (SLHC)

Since especially the interesting high-energy events are very rare at the design luminosity of $10^{34} \text{ cm}^{-2} \text{ s}^{-1}$ and are accompanied by a high QCD background, extracting physically relevant data with reasonable statistics needs a great amount of time. One common example is the search for the Higgs particle; observing the amount of data being required to establish a 5σ discovery, or a 95 % exclusion of the Higgs boson, for example, depends on its invariant mass as shown in figure 1.2.

At the current peak luminosity of about $10^{29} \text{ cm}^{-2} \text{ s}^{-1}$ only data relating to a few fb^{-1} per year are delivered [2]. At the design luminosity of $10^{34} \text{ cm}^{-2} \text{ s}^{-1}$, which will be reached in the year 2017 according to the present upgrade planning, the amount of data will increase up to approximately 60 fb^{-1} every year even though this plan underlies technical feasibility and thereby are varying.

Therefore within 2 - 3 years of collecting data the Higgs boson will be either discovered or entirely excluded over the mass interval [114 GeV, 1 TeV]. This example illustrates the enormous amount of time which is required to collect adequate statistics.

Upgrading the peak luminosity by a factor of ten, as planned, would decrease this time dramatically and therefore would facilitate more detailed measurements of high-energy particles. Major steps to obtain this boost of luminosity are accelerating more protons

1. Introduction

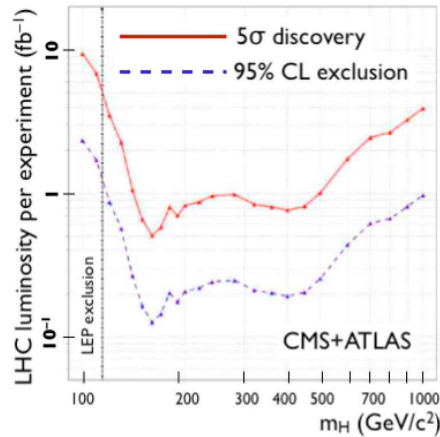


Figure 1.2.: Discovery reach and exclusion limit at the LHC of a Standard Model Higgs boson as function of the Higgs mass[2].

Quantity	LHC	sLHC
Maximum c. m. energy	14 TeV	14 TeV
Design luminosity	$10^{34} \text{ cm}^{-2}\text{s}^{-1}$	$10^{35} \text{ cm}^{-2}\text{s}^{-1}$
No. of bunches per proton beam	2808	2808
No. of collision per second	10^9	10^{10}

Table 1.1.: Important quantities of the LHC and SLHC [7].

per bunch, improved focusing and thereby increasing the average number of pile-up events. In order to exploit those modifications the affected detector experiments ATLAS and CMS have to be adjusted, which becomes clear from figure 1.3. Obviously the raise of luminosity by about two orders increases the numbers of tracks and pile-up events tremendously.

Important quantities and parameters of the LHC and SLHC are summarised and compared in table 1.1.

Section 1.2 discusses the modifications required by the ATLAS experiment in more detail.

1.2. The ATLAS Experiment

With an inelastic proton-proton cross-section of 80 mb at the design luminosity, the LHC will produce 10^9 events per second. Therefore every candidate event for new physics will be accompanied by 23 inelastic events per bunch crossings, which have

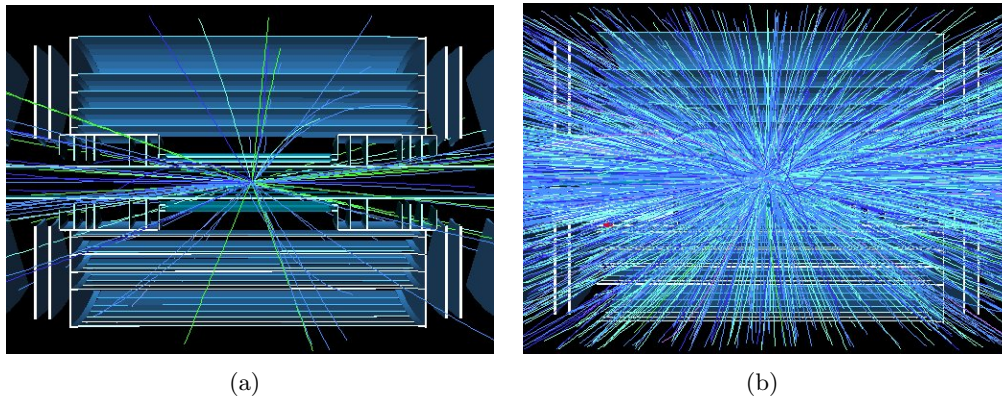


Figure 1.3.: Shown is the same event at two different luminosities as simulated in a proposed candidate of the inner detector the ATLAS experiment; (a) $0.2 \cdot 10^{33} \text{ cm}^{-2} \text{ s}^{-1}$ and (b) $L = 10^{35} \text{ cm}^{-2} \text{ s}^{-1}$, with inclusion of $O(400)$ additional pp interaction during the same bunch crossing [6].

to be identified and filtered. Because of this and other experimental difficulties the detector experiment has to satisfy several physics requirements. Those include fast and radiation hard electronics and sensor modules, a high sensor granularity, high acceptance in pseudo-rapidity¹, a very good charged particle resolution, a high reconstruction efficiency as well as an excellent calorimetry- and muon detection system. A highly efficient trigger-system in order to reject uninteresting events with a low transverse momentum is of equal importance.

The ATLAS (A Toroidal LHC Apparatus) experiment - one of six detector experiments located at the Large Hadron Collider (LHC) - meets those requirements.

1.2.1. Basic Design of ATLAS

The ATLAS experiment is basically designed as a general-purpose detector. Several detection systems provide detailed track and energy information of produced particles.

Figure 1.4 shows the ATLAS detector and indicates its tremendous dimensions; the forward-backward symmetric detector is 25 meters high and 44 meters long with an overall weight of 7000 tons.

¹**Pseudo-rapidity** $\eta = -\ln(\tan \frac{\Theta}{2})$ is used as a spatial coordinate, which depends on the angle Θ between the particle direction and the beam direction.

1. Introduction

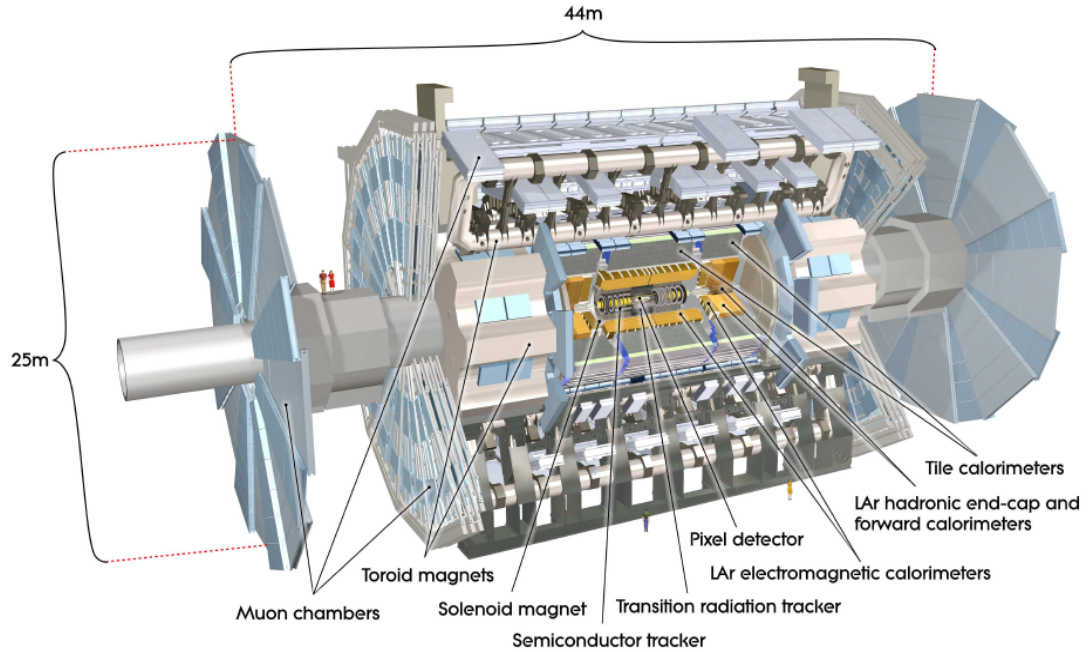


Figure 1.4.: Cut-away view of the ATLAS experiment[1].

The Magnet System

The ATLAS magnet system consists of a superconducting solenoid, surrounding the inner detectors with a magnetic field of 2 T in beam direction, and eight superconducting coils (barrel toroid) (cf. figure 1.5) and two end-cap toroids. The latter provide toroidal magnetic fields mostly orthogonal to the muons trajectory of approximately 0.5 T.

Inner Detector

The Inner Detector (ID) of the ATLAS experiment is composed of three independent complementary sub-detectors as shown in figure 1.5.

- three cylindrical **silicon pixel**-layers with individual sensor-elements with a granularity of $50\ \mu\text{m} \times 400\ \mu\text{m}$ provide a high resolution pattern recognition capability
- additionally four stereo pairs of silicon micro-strip layers (**SCT**) with a pitch of $80\ \mu\text{m}$ in Φ -direction, 12 cm length in beam-direction and $250\ \mu\text{m}$ thickness in r -direction facilitate track reconstructions. In order to increase the detector resolution in beam direction, the individual layers of a stereo pair are tilted

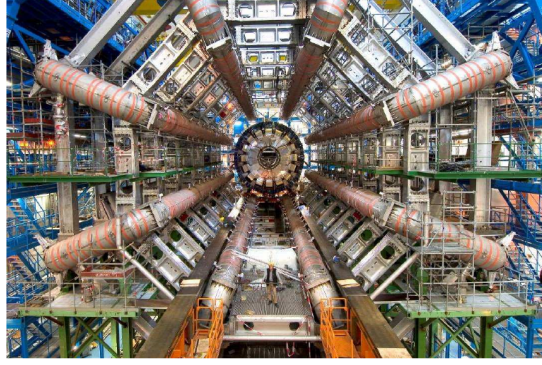


Figure 1.5.: Shown are the eight barrel toroid coils as installed in the underground cavern. They induce a toroidal magnetic field of 0.5 T, which enclosed the muon detector[1].

towards each other by 45 mrad. The distance between those two layers is 0.45 cm.

- the transition radiation tracker (**TRT**) separates electrons from pions due to their transition radiation. Additionally it enhances the pattern recognition, by adding continuous tracks, since a traversing particle generates on average 36 hits on the correspondent gaseous straw tube elements.

It is designed to provide detailed track information of charged particles and to cover a wide pseudo-rapidity range of $|\eta| < 2.5$ as well as a broad transverse momentum range of $0.5 \text{ GeV} < p_T < 150 \text{ GeV}$.

Because of the expected radiation exposure, the inner pixel layer will have to be replaced at the latest after collecting data of 300 fb^{-1} .

Calorimetry

In order to meet the physics requirements of jet reconstruction and E_T^{miss} detection the calorimetry of the ATLAS detector comes with a hadronic calorimeter system covering a pseudo-rapidity range of $|\eta| < 4.9$ and an electromagnetic calorimeter system having a fine granularity for precision measurements of electron and photon energies. Especially for the search for the Higgs boson (cf. 1.1.2) the latter are important and therefore need to be measured very precisely. One of those important decay channels of the Higgs boson is the following: $H \rightarrow ZZ \rightarrow e^-e^-e^-e^-$.

The **electromagnetic calorimeter system** is based on a lead-liquid argon (LAr) calorimetry technology. The accordion-geometry ensures full coverage in Φ . The thickness of the lead absorbers varies as a function of η in order to obtain the optimum performance in energy resolution.

1. Introduction

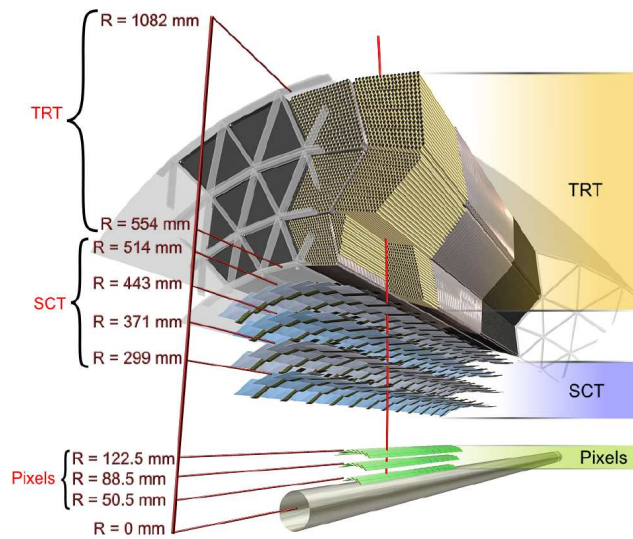


Figure 1.6.: Illustration of the three detection components of the inner detector[1].

In addition to the LAr electromagnetic calorimeter barrel, two LAr electromagnetic end-cap calorimeters (EMEC) help to expand the pseudo-rapidity range.

The **hadronic calorimeter system** is composed of the tile calorimeter, the LAr hadronic end-cap calorimeter (HEC) and the LAr forward calorimeter (FCal).

The tile calorimeter envelops the electromagnetic calorimeter and uses steel as the absorber and scintillating tiles as the active material.

Muon System

The muon spectrometer is designed to detect charged particles exiting the calorimetry system and to measure their transverse momenta. It covers a pseudo-rapidity range of $|\eta| < 2.7$.

Figure 1.8 shows several kinds of straw chambers: the thin-gap chambers (TGC), resistive plate chambers (RPC), cathode strip chambers (CSC) and the monitored drift tubes (MDT). The location of those different straw chambers are determined due to their individual specifications such as granularity or radiation resistance for instance.

Trigger System

Currently the ATLAS detector uses a trigger system, which is composed of three levels; the level 1 trigger (L1), the level 2 trigger (L2) and the event filter. Each level refines

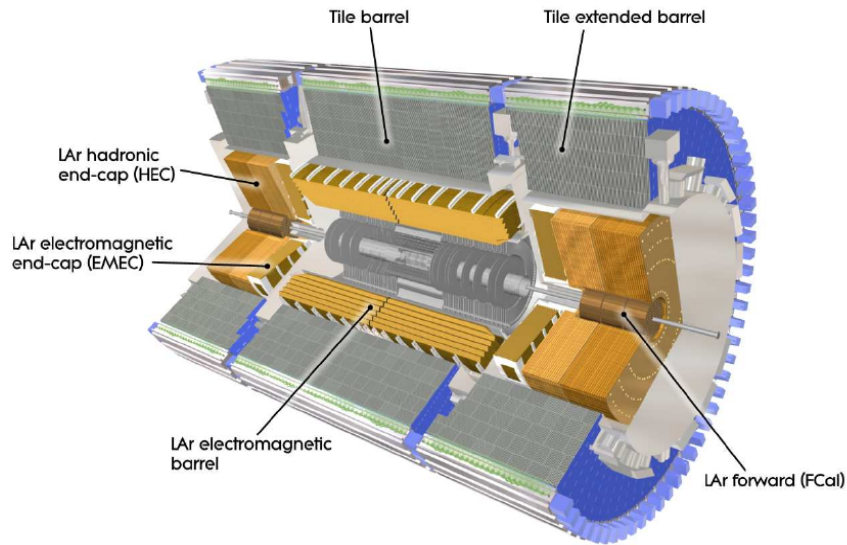


Figure 1.7.: Cut-away view of the ATLAS calorimeter-systems [1].

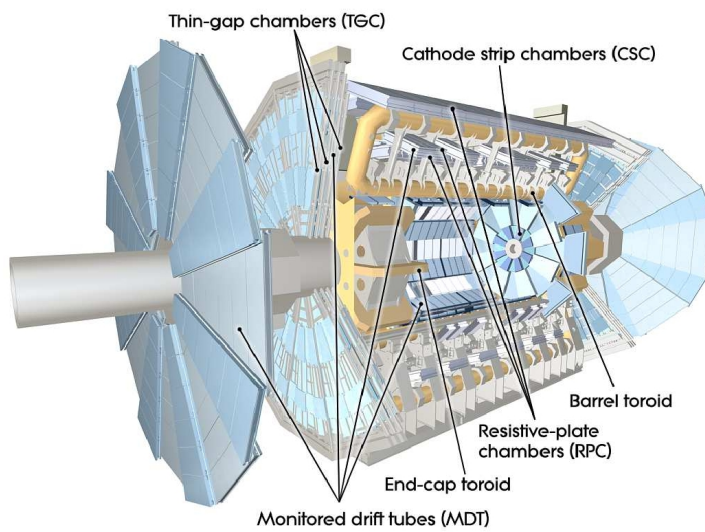


Figure 1.8.: Cut-away view of the ATLAS muon spectrometer [1]. Several chambers are utilised for detecting traversing charged particles.

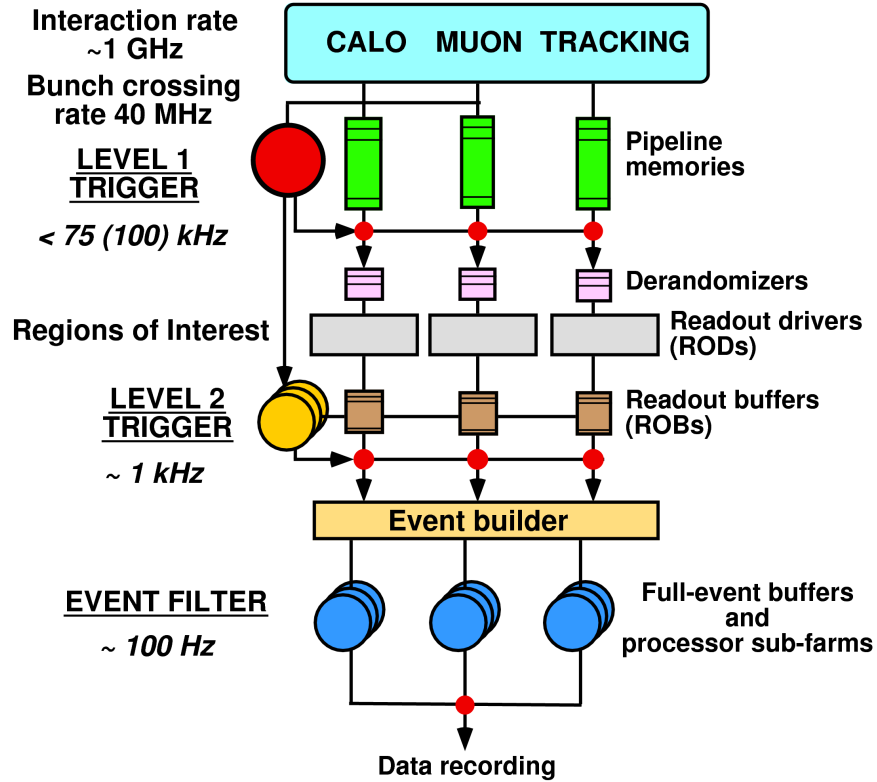


Figure 1.9.: Diagram of the ATLAS trigger system. L1 reduces the event rate from 40 MHz to <math>< 75 \text{ kHz}</math>. In the next steps the high level triggers (HLT) decreases the event rate down to 100 Hz [1].

the decision made by the previous level by using a greater amount of information from the detector and thereby decreasing the event rate.

The diagram shown in figure 1.9 illustrates the functionality of the ATLAS trigger system and its reduction potential. While L1 is completely implemented in hardware L2 and the event filter, which form the high level trigger (HLT), are mainly implemented in software and runs on commercial computers and network devices.

The L1 decision is based on information from the first level muon spectrometer (L1Muon) and the calorimetry-system (L1Calo). By using reduced granularity information from the RPC and TPC of the muon system 1.2.1 as well as the electromagnetic calorimeter, the trigger looks for high energetic muons, electrons, photons, jets², τ -leptons decaying into hadrons and events with a large amount of missing Energy E_T^{miss} . Thereby L1 reduces the event rate from 40MHz to <math>< 75 \text{ kHz}</math>.

²A **jet** is a narrow cone of hadrons and other particles produced by the hadronisation of quarks or gluons, which are originated from hard scattering.

As shown in figure 1.9 L1 defines regions of interest (RoI) to the next trigger level within 2.5 μs . These regions of the detector form possible trigger objects, which are further evaluated at higher trigger levels. The HLT-algorithms utilise the full granularity and precision of the data from the calorimeters, muon chambers and the inner detector to reduce the event rate to a few 100 Hz.

1.3. The ATLAS High Luminosity Upgrade

Since the planning of the ATLAS Upgrade has not been finished yet, the following will only provide information of the problems caused by the increment of luminosity and actual design ideas to solve them with focus on the ID and trigger system.

1.3.1. Inner Detector

Because of radiation damage it was evident on early, that the ID would be replaced by its entirely after collecting data of approximately 300 fb^{-1} due to radiation damages of the detector. The current expectation is that the ID will become an all-silicon system [8], i. e. the TRT-system will be replaced by a silicon-system as shown in figure 1.10.

Furthermore, other processes, such as optimising the chipdesign for radiation hardness for instance, are on their way.

1.3.2. ID Design Planning

Figure 1.10 also shows the parameters of the SCT detectors. They will differ by their length, while their pitch will be staying constant; at larger radii long silicon strips of 10 cm length will be used. In order to increase the granularity, the length of the inner strip layers as well as the pixel detectors will be decreased to 2.4 cm and 250 μm , respectively. The stereo structure of the SCT is planned to be retained.

As shown in figure 1.11 the individual SCT-layers are not cylindrically but cylindrical-symmetrically distributed among the beam pipe.

There are three distinct radial regions; the innermost barrel includes the inner b -layer and three silicon pixel-layers out to a radius of 28 cm. The middle region extends to a radius of 60 cm and contains three layers of short SCT-strips. The outer region begins at a radius of 60 cm and includes two layers of long SCT-strips.

1. Introduction

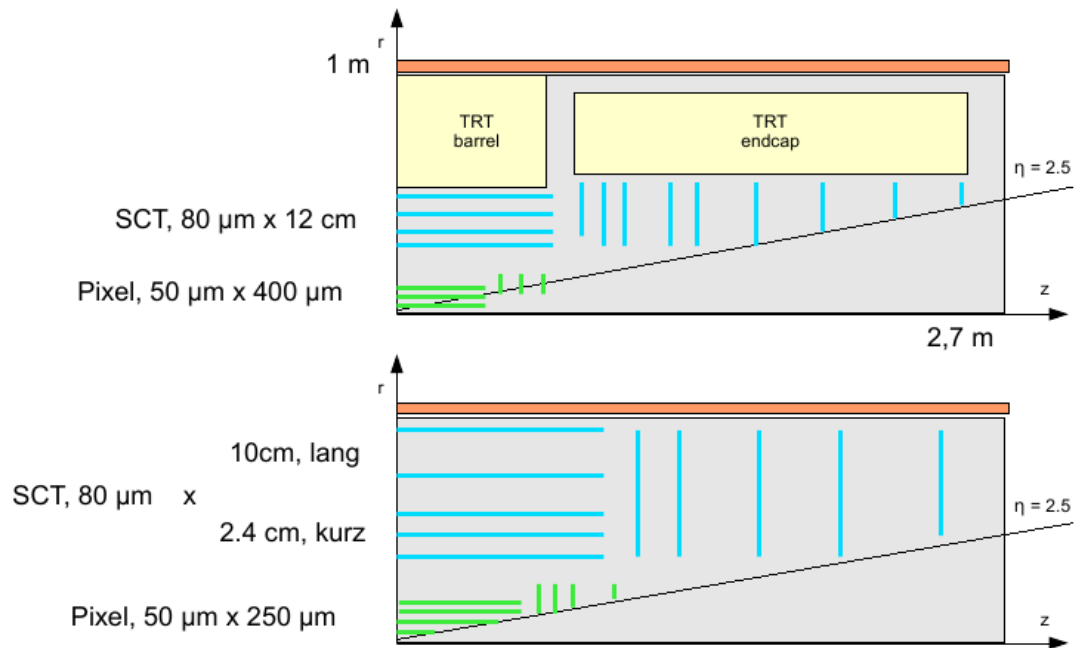


Figure 1.10.: Comparison between the current (upper figure) and one possible design (lower figure) for the new ID of the ATLAS experiment. The actual TRT-system becomes replaced by silicon-detectors.

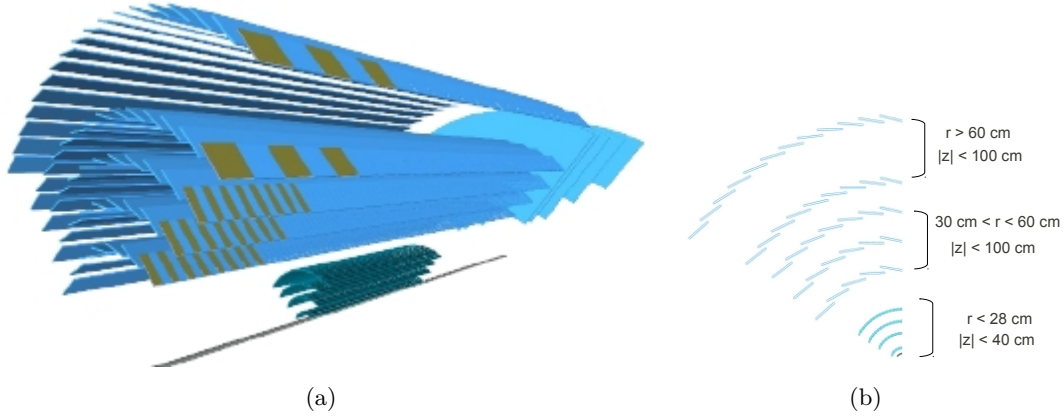


Figure 1.11.: Three dimensional view (a) and profile view (b) of a planned design of the ID of the ATLAS detector.

Results of Geant4 [9] predict an occupancy³ of 2% on the innermost SCT-layer ($r = 38$ cm) at the anticipated luminosity of 10^{35} $\text{cm}^{-2}\text{s}^{-1}$.

1.3.3. L1 Trigger System

The planned increment of luminosity will challenge the L1 trigger-system in two ways.

One major problem is the increased particle density, which leads to a higher occupancy. Therefore a much larger data volume has to be read out from the detector. The other problem is the expected increase of trigger rates by an order of magnitude under the constraint of constant p_T -thresholds.

Hence the L1 trigger system is expected to be improved and complemented with several features. Apart from enabling the L1Calo access to full granularity, adding track information from the ID to refine the trigger decision, i. e. adding a L1 track trigger, is the most promising technique to overcome the problems mentioned above.

Regional Readout

As described in section 1.3.2 it is planned to increase the ID granularity. Hence even more channels would have to be read out, which is simply not feasible at 40 MHz. A regional read out of Regions of Interest (RoI)[10] would solve this problem.

The main idea is to use information given by L1Calo and L1Muon to define RoIs (ϕ, η) and relay them to the L1 track trigger. Therefore only a fraction of all channels has to be read out. Figure 1.12 shows the RoI for a detected lepton.

³The ratio of the number of detected interactions between individual detector-strips and the overall number of strips per detector barrel is referred to as **occupancy**.

1. Introduction

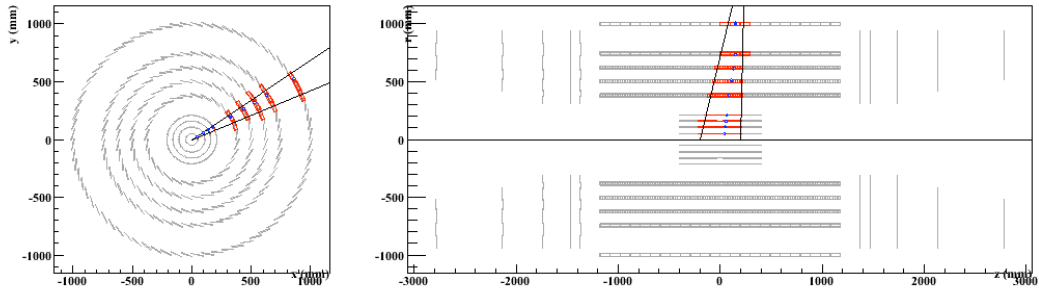


Figure 1.12.: A lepton RoI in the ID, in the x - y and the ρ - z projections. The RoI is wider in z close to the beam line to account for the spread of the luminous region in z [11].

Correlations of Double Layers

Another approach to reduce the data volume is exploiting the double layer structure of the SCT to select hits from high- p_T particles only.

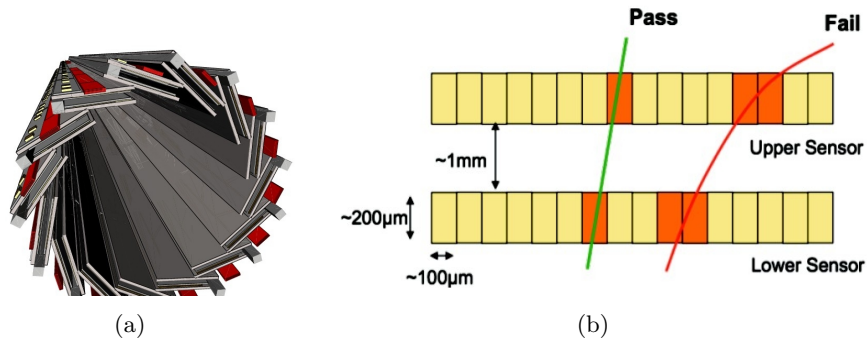


Figure 1.13.: Shown are a three dimensional illustration of an inner detector barrel of the CMS experiment (a) and a closer view on two particles traversing one individual SCT element (b).

Figure 1.13.a shows the architecture of double layer detector. Figure 1.13.b shows a $r - \phi$ -profile view of a single double layer detector and illustrates the idea behind using the double layer structure to determine the transverse momentum of a particle; because of the surrounding magnetic field in beam direction a charged particle is accelerated on a circular trajectory, whose curvilinearity depends on the the transverse momentum of the particle. Particles with a low transverse momentum are deflected more than those with a high transverse momentum.

1.3. The ATLAS High Luminosity Upgrade

Hence the distance between the interaction on the inner layer and the hit on the outer layer depends inversely on the transverse momentum of the particle. This relation can be used to filter particles with a low transverse momentum.

This method is pursued as the baseline by CMS. Correspondent studies for the ATLAS detector will be the subject of this thesis.

1. Introduction

2. Monte Carlo Software

In the following studies idealised detector quantities are used in order to quantify filter and reconstruction possibilities offered by the double layer-detector structure in a very fundamental way.

Therefore a toy Monte Carlo is utilised, which rapidly simulates events and corresponding particle tracks. The idealised detector architecture ensures a focus on the basic problems of this idea.

This chapter describes important quantities, such as the generated distribution of the transverse momenta of the particles (cf. section 2.2.1), which form the groundwork of the following studies.

2.1. Idealised Detector Architecture

Figure 2.1 shows the idealised detector architecture, which will be studied in this thesis; three 2.4 m long double-layer SCT detector barrels, whose individual silicon-strips have a pitch of 80 μm in ϕ -direction and an extension of 2.4 cm in beam direction. End-caps are not taken into account.

The whole ID is surrounded by an magnetic field of 2 T in beam-direction (cf. section 1.2.1).

2.2. Framework of Simulations

In the used simulations the toy Monte Carlo is set to generate one event producing 50,000 tracks in order to reach the expected occupancy of 2 % on the inner most SCT. Each particle induces only one hit on the detector barrel per crossing, even though an individual particle with a low transverse momentum can cross a barrel several times, since it is deflected on a helix trajectory.

Effects of interactions between particles and matter such as multiple scattering and energy losses are also taken into account by the toy Monte Carlo, where the energy loss is based on the Bethe-Bloch-formula[12].

2. Monte Carlo Software

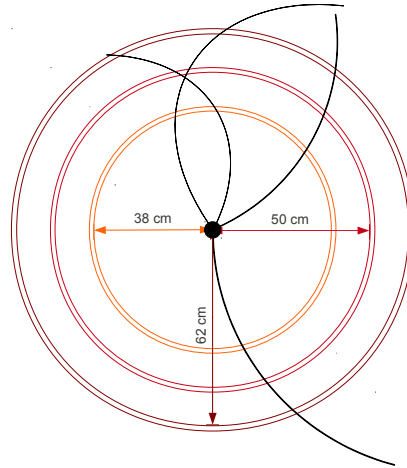


Figure 2.1.: View in beam direction of the idealised cylindrical-symmetric detector architecture used by the Monte Carlo simulations. Shown are three SCT barrels with the inner radii 38 cm, 50 cm and 62 cm. The distance between two layers of of a SCT barrel is 0.45 cm.

2.2.1. p_T Distribution

The distribution of the transverse momenta p_T of the particles shown in figure 2.2 was generated according to a PYTHIA6[13] 14 TeV proton-proton minimum-bias simulation.

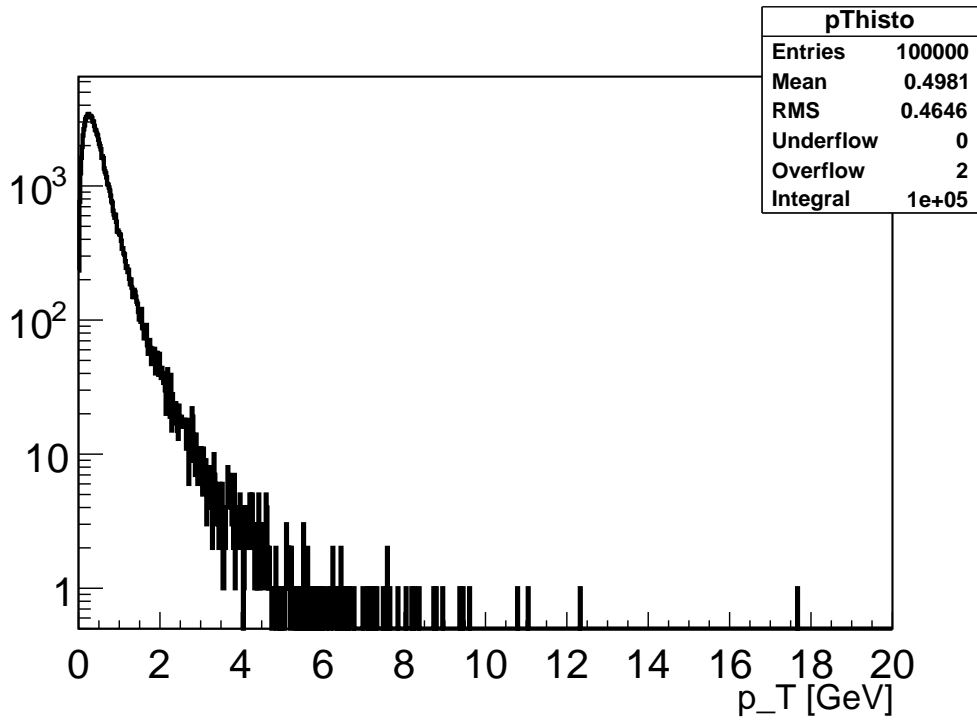


Figure 2.2.: p_T distribution according to a PYTHIA6 14 TeV proton-proton minimum-bias simulation.

2. Monte Carlo Software

3. Geometry

In the first section of this chapter the relation between the transverse momentum of a particle p_T and the offset, i. e. the difference in cell number Δn of the interactions the particle causes on both layers of a double layer detector, is quantified for the transverse plane.

The second section concerns the x - z plane. Although the offset in z -direction is not used to obtain information about the transverse momentum of a particle, it is necessary to study its distribution. Those information are needed to set limits for correct particle interaction assignments.

3.1. Trajectory in the Transverse Plane

In order to determine the dependence of the difference in cell number $\Delta n = \frac{\Delta x}{a}$ between the two layers of a double layer detector from the transverse momentum p_T of the particle in the magnetic field B , one can use the following geometrical consideration.

Due to Lorentz-forces the particle moves along a circle in the transverse plane with a radius r depending on the magnetic field B and the transverse momentum p_T of the particle:

$$r = \frac{p}{cqB} \quad (3.1)$$

Since the dependence of the chords R_i from the radius r and the apex angles α_i is given

$$R_i = 2r \sin \alpha_i \quad (3.2)$$

one gets

$$\alpha_i = \arcsin \frac{R_i}{2r} \quad (3.3)$$

Figure 3.1 shows the connection between the apex angles α_c , α_1 and α_2

$$\alpha_c = \alpha_2 - \alpha_1 \quad (3.4)$$

$$= \arcsin \frac{R_2}{2r} - \arcsin \frac{R_1}{2r} \quad (3.5)$$

3. Geometry

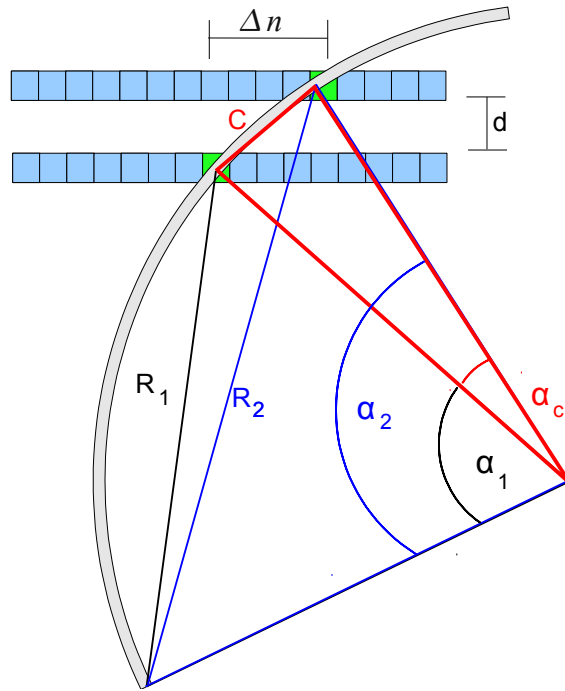


Figure 3.1.: Particle moves along a circle and crosses the double-layer detector with an offset corresponding to its transverse momentum. This figure illustrates the way of thinking and is not true to scale.

3.1. Trajectory in the Transverse Plane

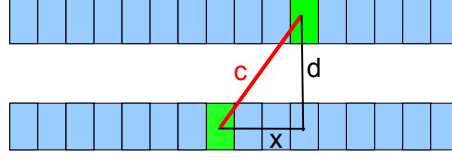


Figure 3.2.: The chord c is the hypotenuse of a right angled triangle.

thus

$$c = 2r \sin \left(\arcsin \frac{R_2}{2r} - \arcsin \frac{R_1}{2r} \right) \quad (3.6)$$

$$= 2r \left[\frac{R_2}{2r} \cos \arcsin \frac{R_1}{2r} - \frac{R_1}{2r} \cos \arcsin \frac{R_2}{2r} \right] \quad (3.7)$$

$$= R_2 \sqrt{1 - \left(\frac{R_1}{2r} \right)^2} - R_1 \sqrt{1 - \left(\frac{R_2}{2r} \right)^2} \quad (3.8)$$

Because of c being also the hypotenuse of the right angled triangular¹ shown in figure 3.2 Δx can be determined by using the Pythagorean theorem, since the distance $d = R_2 - R_1$ between the two layers is known².

$$\Delta x = \pm \sqrt{c^2 - d^2} \quad (3.9)$$

$$= \pm \sqrt{\left[R_2 \sqrt{1 - \left(\frac{R_1}{2r} \right)^2} - R_1 \sqrt{1 - \left(\frac{R_2}{2r} \right)^2} \right]^2 - d^2} \quad (3.10)$$

$$= \pm \sqrt{\left[(R_1 + d) \sqrt{1 - \left(\frac{R_1}{2r} \right)^2} - R_1 \sqrt{1 - \left(\frac{R_1 + d}{2r} \right)^2} \right]^2 - d^2} \quad (3.11)$$

thus

$$\Delta n = \pm \frac{\sqrt{\left[(R_1 + d) \sqrt{1 - \left(\frac{R_1 c q B}{2p} \right)^2} - R_1 \sqrt{1 - \left(\frac{(R_1 + d) c q B}{2p} \right)^2} \right]^2 - d^2}}{a} \quad (3.12)$$

In order to check equation 3.12 for accuracy the toy Monte Carlo is set to only generate tracks with certain transverse momentum. The offset distribution of such a Monte Carlo simulation is shown in figure 3.3. The mean value and the according rms are plotted in figures 3.4 and 3.5.

According to figures 3.4 and 3.5 this equation is consistent with the results of the simulation even so material effects have not been taken into account. Since $\Delta n \in \mathbb{Z}$

¹This implies that the layers are approximately parallel, which is given as long as $\Delta x \ll R_1$.

² $d = R_2 - R_1$ is a first order approximation under the assumption of R_i being perpendicular to the layers. Here it can be used since $\Delta x \ll R_1$

3. Geometry

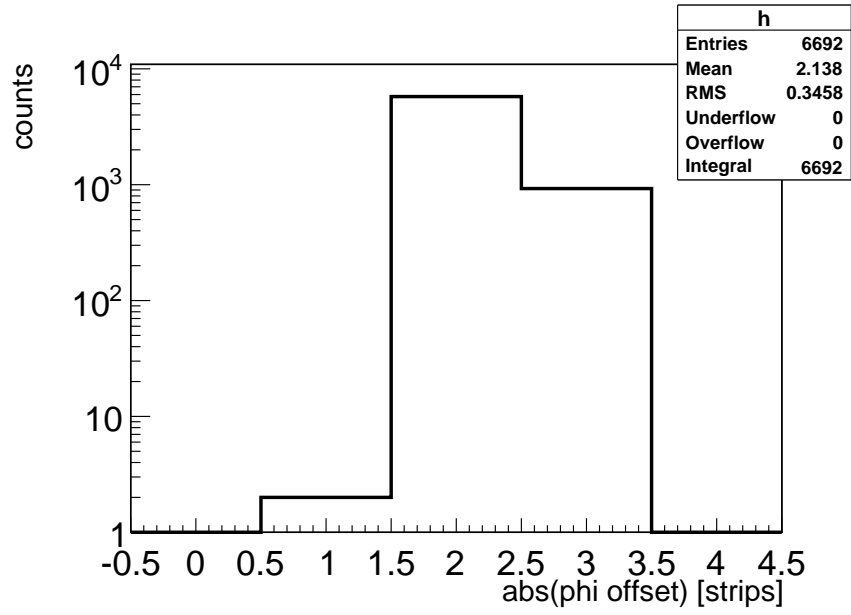


Figure 3.3.: Offset distribution of a toy Monte Carlo simulation, which produced 10,000 events with a transverse momentum of 3 GeV.

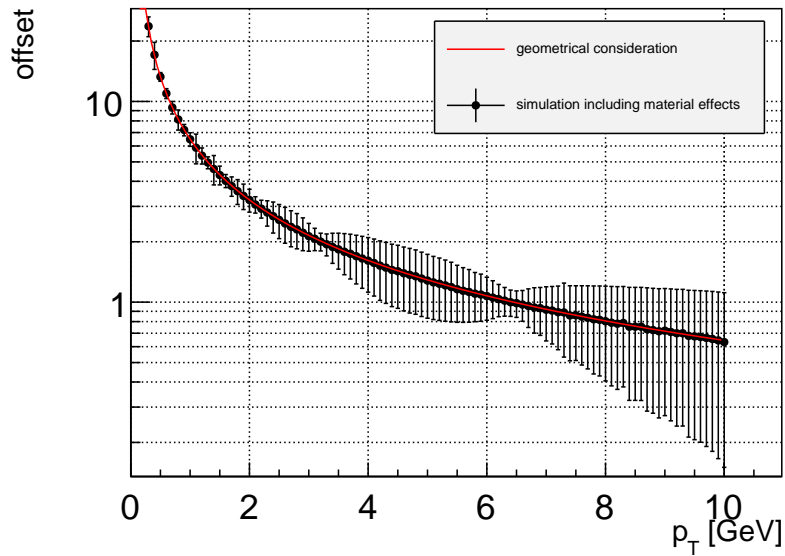


Figure 3.4.: Shown is equation 3.12 in comparison with results of the simulation. Both use the parameters $R_1 = 38$ cm, $d = 0.45$ cm, $a = 80$ μ m, $B = 2$ T and $q = e$. The shown errorbars relate to the rms of the offset distribution of each simulation.

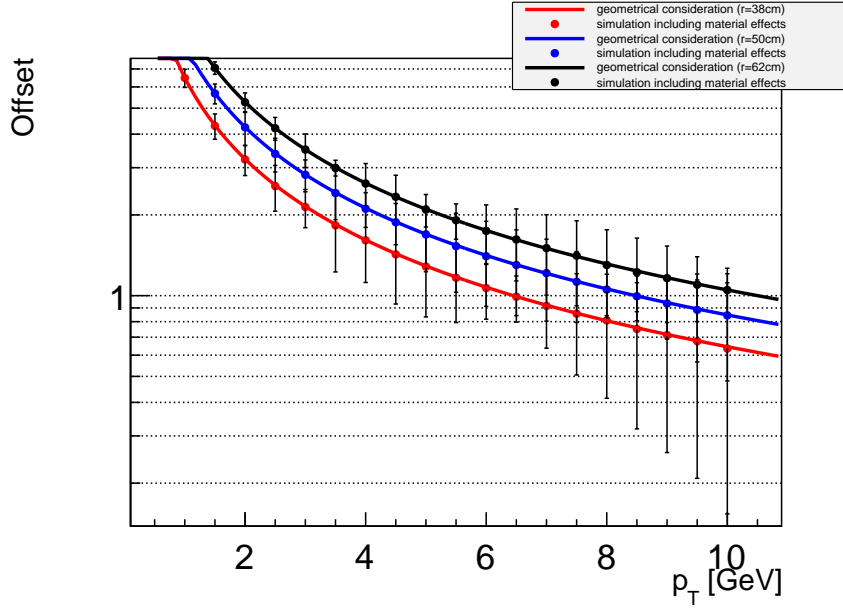


Figure 3.5.: Shown is equation 3.12 in comparison to the results of the simulation for all three radii given by the experimental setup.

discretisation effects become dominant for particles with a high transverse momentum p_T .

3.2. Offset in z -Direction

Although the silicon-strips are 2.4 cm long, the pattern recognition will also have to take an offset in z -direction into account; otherwise there will be a loss of particles of approximately 24.7 % according to figure 3.6. Obviously an offset range of $|\Delta z| \leq 1$ would be sufficient.

3. Geometry

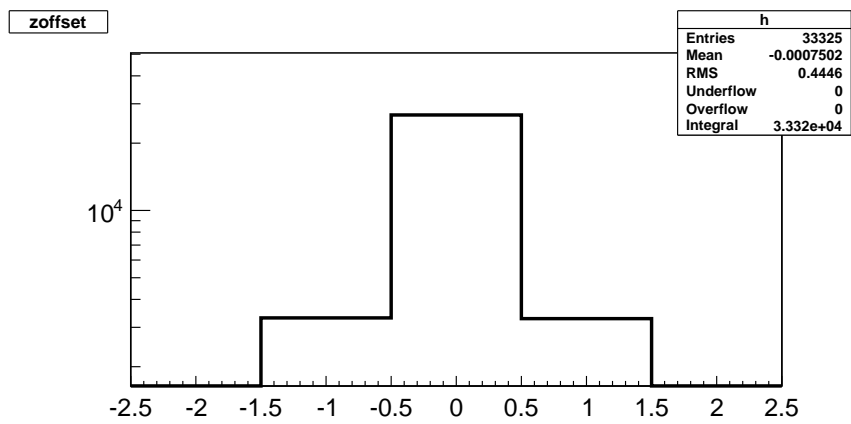


Figure 3.6.: Offset distribution in z -direction between the individual layers of a SCT-barrel. Approximately 24.7 % of all particles have an offset $|\Delta z| > 0$.

4. Combined Algorithm

In this chapter two algorithms are used to illustrate the main idea behind exploiting the double layer structure to reduce the amount of tracks (cf. section 4.1 and to reconstruct hits (cf. section 4.2), which have gone lost due to single-hit-inefficiencies of the silicon-strips.

4.1. Selection of High Transverse Momentum Candidates

In a first step an algorithm is implemented, which is capable of finding candidates for particles with a transverse momentum above a given cut. The algorithm searches for coincidences (cf. A), i. e. a pair of hits on the double layer detector, which may origin from the same particle, and returns those, which have a small offset in ϕ -direction. Since small offsets correspond to small deflections of high transverse momentum particles in the magnetic field, all returned coincidences are trigger candidates.

Technically spoken the algorithm uses equation 3.12 to calculate an offset, which corresponds to the applied high transverse momentum cut. Because of the possible offset in z -direction $|\Delta z| \leq 1$ (cf. section 3.2) the search region becomes two dimensional.

For each hit on one layer the two dimensional search region¹

$$(\Delta n, \Delta z) \in [-(\Delta n(p_T^{\text{he-cut}}) + 1), \Delta n(p_T^{\text{he-cut}}) + 1] \times [-1, 1]$$

on the opposed layer is scanned. If the algorithm finds a hit inside this region, it will return the coincidence as a high transverse momentum candidate.

Figure 4.1 illustrates the modus operandi of this algorithm.

In this example a high- p_T cut of 8 GeV is applied. Since the double layer detector at $r = 38$ cm is observed equation 3.12 returns a corresponding offset region of $|\Delta n| = 0$.

Because of the additional offset in z - and ϕ -direction, the actual search region becomes $(\Delta n, \Delta z) \in [-1, 1] \times [-1, 1]$.

¹The additional strip in ϕ -direction has to be taken into account since equation 3.12 only returns the mean value of the offset. Therefore particles with an offset $\Delta n(p_T^{\text{he-cut}}) + 1$ are also possible trigger candidates.

4. Combined Algorithm

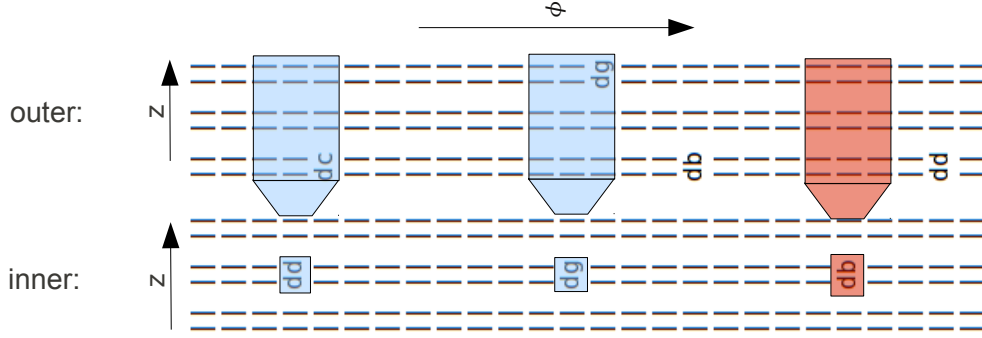


Figure 4.1.: Illustration of the mode of operation of the algorithm for selecting high transverse momentum candidates.

For each hit on the inner layer the algorithm scans the search region on the opposed layer. If it finds an interaction inside this region, it will consider the corresponding coincidence as induced by a particle with a high transverse momentum (blue).

In the case of the g -particle this assignment is correct, because the hit, which is found in the search region of the d -particle, corresponds to another particle c . Therefore this is a fake coincidence, which mimics to be induced by a high- p_T particle.

Obviously the transverse momentum of particle b does not meet the cut-condition. Therefore no interaction is found inside the search region on the outer layer (red). This interaction is not considered ob being a part of a coincidence induced by a high energetic particle.

4.1.1. Reduction of Data Volume

As shown in illustration 4.1 not only particles with a high transverse momentum but also fake coincidences of two different low energetic particles are considered as trigger objects. In fact most of the returned trigger candidates are from the latter kind.

While only a small fraction $< 0.5\%$ (cf. figure 2.2) of all particles have a transverse momentum above 7.2 GeV, figure 4.2.a indicates that this algorithm

The main reason for this amount of fake coincidences is the great number of particles with a low transverse momentum, which aggravate right hit associations. There is no way to avoid those fake coincidences, since all of them meet the same requirements as a coincidence induced by a particle with a high transverse momentum.

As shown by figure 4.2.c an even better data reduction can be obtained at higher radii. This has two reasons. The first reason is the lower occupancy ($< 1\%$). The second reason is that particles with a very low transverse momentum do not reach this double layer detector (cf. section A.5).

4.1. Selection of High Transverse Momentum Candidates

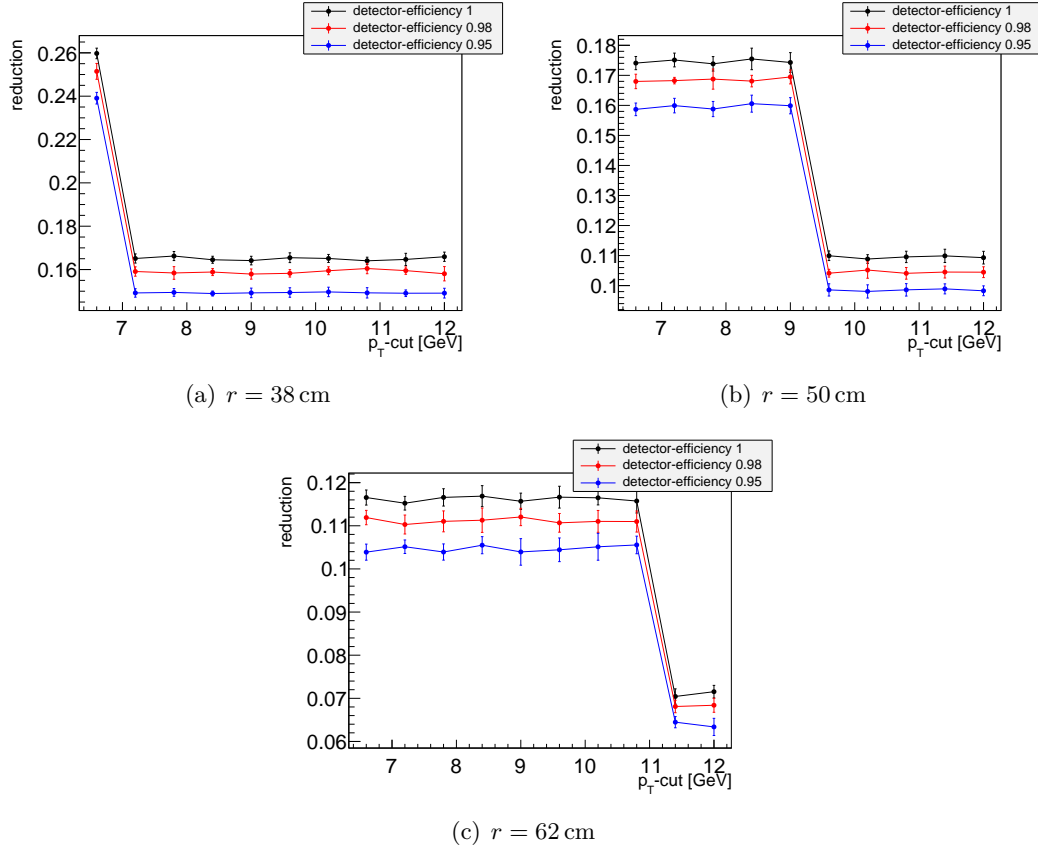


Figure 4.2.: Plot of the reduction of information obtained by the algorithm with respect to the underlying p_T cut for three different detector radii. Each plot shows the results of three simulations with different single-hit-efficiencies of the detector. The characteristic reduction step is the result of the offset resolution, which is determined by the double layer design. In this case shown is the step from the search interval $(\Delta n, \Delta z) \in [-2, 2] \times [-1, 1]$ to $(\Delta n, \Delta z) \in [-1, 1] \times [-1, 1]$.

4. Combined Algorithm

4.1.2. Efficiency

As shown by figure 4.3 this algorithm finds almost all particles with a transverse momentum above the applied cut at full single hit efficiency of the detector-strips ($\epsilon_{det} = 1$). Due to multiple scattering and other boundary effects the algorithm does not reach 100 % efficiency at each run.

Figure 4.3 also shows that the algorithm efficiency ϵ_{alg} declines quadratically with respect to the single hit efficiency of the detector ϵ_{det} as expected. This behaviour is the result of both layers being equally inefficient. If only one of both interactions between a particle with a high transverse momentum and the SCT is not detected the algorithm will not find it. The probability for one interaction becoming lost is given as follows:

$$\epsilon_{alg} \simeq \epsilon_{det}^2$$

4.2. Reconstruction of Lost Hits

Due to single hit inefficiencies of the SCT some interactions between silicon-strips and particles are not detected. Hence, the next step is to consider those single hit inefficiencies in order to avoid losing interesting particles with a high transverse momentum. The main idea to reconstruct those tracks is to exploit the absence of a hit on the opposed layer.

A particle has to have at least a minimum transverse momentum to reach the double layer detector. Therefore the offset in ϕ -direction of a coincidence has an upper border (cf. A.5), which is referred to as maximum search offset. It can be calculated by using equation 3.12.

Hits, which have no possible associated hit on the opposed layer within this maximum search offset, are referred to as isolated hits (cf. section A). The corresponding hit on the opposed layer must have gone lost due to a single-hit inefficiency of the silicon-strip-detector. Therefore the underlying hit is considered to be part of a coincidence induced by a high- p_T particle.

In a more technical manner: The algorithm calculates the maximum search offset corresponding to the radius of the SCT. Afterwards for each hit it scans the search region corresponding to the maximum search offset (cf. A.5) on the opposed layer:

$$(\Delta n, \Delta z) \in [-(\Delta n_{max} + 1), \Delta n_{max} + 1] \times [-1, 1]$$

If it does not find a hit inside this region the algorithm declares the underlying hit as an interaction induced by a particle with a high transverse momentum. Certainly, only a small fraction of those hypothetical trigger candidates are really induced by a

4.2. Reconstruction of Lost Hits

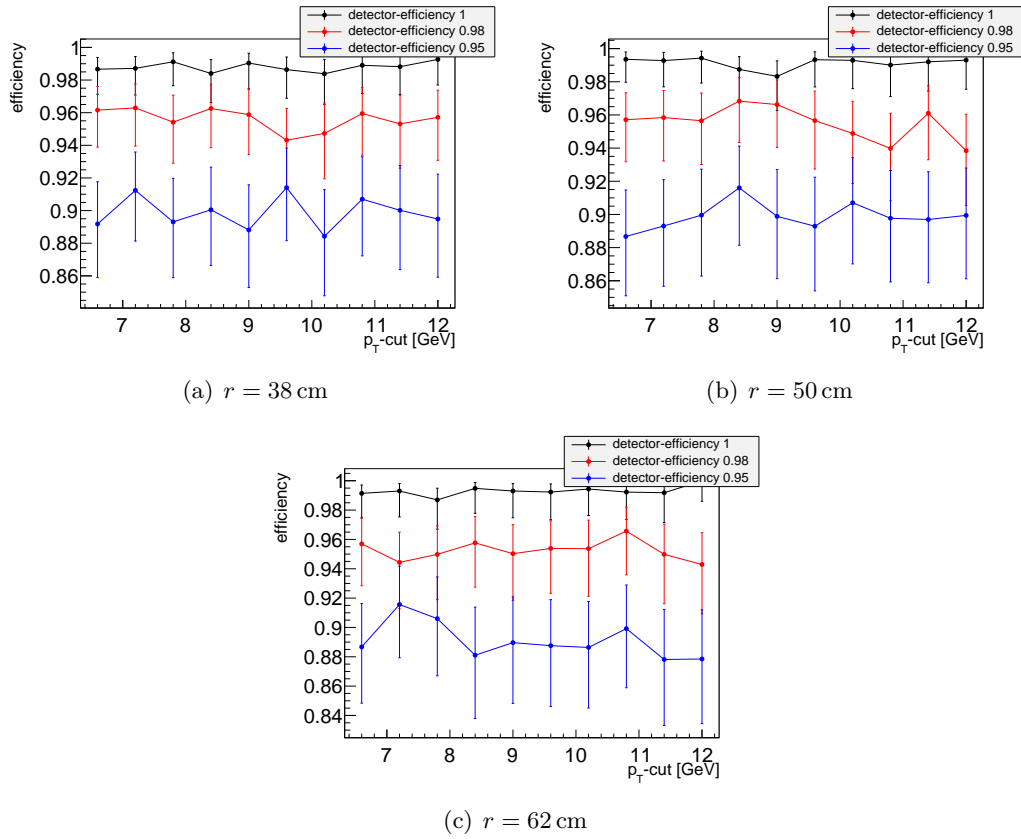


Figure 4.3.: Plot of the algorithm efficiency with respect to the underlying p_T cut for three different detector radii. Each plot shows the results of three simulations with different single-hit-efficiencies of the detector.

4. Combined Algorithm

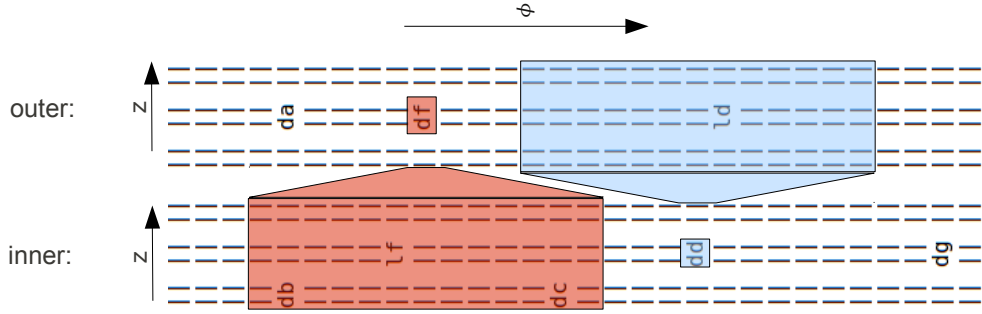


Figure 4.4.: Illustration of the mode of operation of the reconstruction algorithm.

high- p_T particle. However, there are no additional information, which could be used to decide whether or not to consider the isolated hit as induced by an interesting particle.

Figure 4.4 illustrates the mode of operation of the reconstruction algorithm.

In this example the maximum search offset is $\Delta n = 5$. Therefore the corresponding maximum search region is $(\Delta n, \Delta z) \in [-6, 6] \times [-1, 1]$. For each hit the algorithm searches on the opposed layer for detected interaction inside the maximum search region. The illustration demonstrates this procedure for two interactions, whose associated hit is lost.

The high- p_T f -particle for instance is not returned as a trigger candidate (red), since two hits (db and dc) are located inside the maximum search region on the opposed layer and mimic possible associated hits.

However, the particle d is correctly reconstructed by the algorithm (blue), since no interaction on the opposed layer inside the maximum search region is found.

4.3. Combined Algorithm

In the following the performance in efficiency and data reduction of the combination of both presented algorithms is shown and discussed. Combining the algorithms means that all high- p_T candidates found by the reconstruction algorithm are added to those returned by the algorithm for selecting high- p_T candidates.

4.3.1. Efficiency

Figure 4.5 shows the efficiencies of the combined algorithm for different radii of the detector. For each radius three different single-hit-inefficiencies are applied.

Compared to the plots of the efficiency of the algorithm, which selects complete high- p_T coincidences (cf. 4.1), no remarkable difference can be observed. Obviously the

4.3. Combined Algorithm

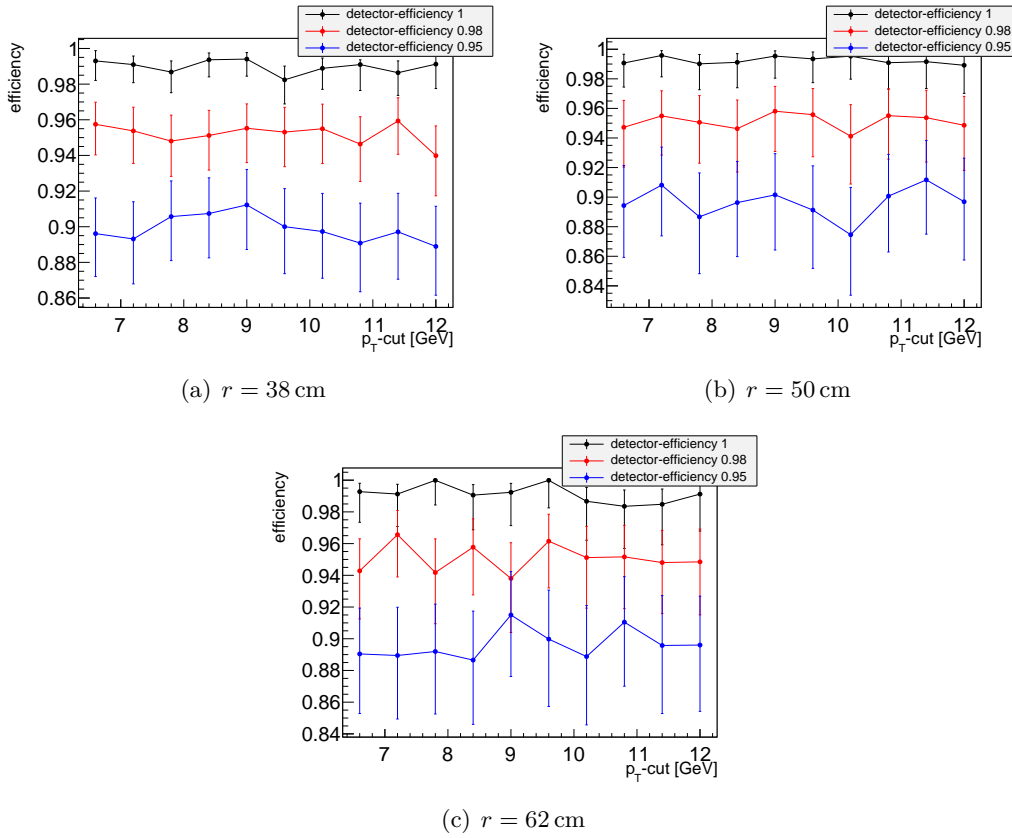


Figure 4.5.: Plot of the algorithm efficiency with respect to the underlying p_T cut for three different detector radii. Each plot shows the results of three simulations with different single hit efficiencies of the detector.

presented algorithm for hit reconstruction is not capable of improving the efficiency significantly.

Even for the most outer layer at $r = 62$ cm no difference between the first and the combined algorithm appears. This may appear unexpected, since the occupancy of this detector-barrel is located below 1%. But the following calculation shows, that even this occupancy prevents the reconstruction of lost hits.

At $r = 62$ cm equation A.1 returns $p_{T_{min}} = 187$ MeV. The corresponding maximum search offset is $|\Delta n_{max}| \approx 800$. Therefore even though on only one of a hundred strips an interaction is detected, on average 16 interactions² lie inside its maximum search offset on the opposed layer. Hence almost no interaction can be considered of being an isolated hit.

²The maximum search offset is scanned in positive and negative direction of ϕ .

4. Combined Algorithm

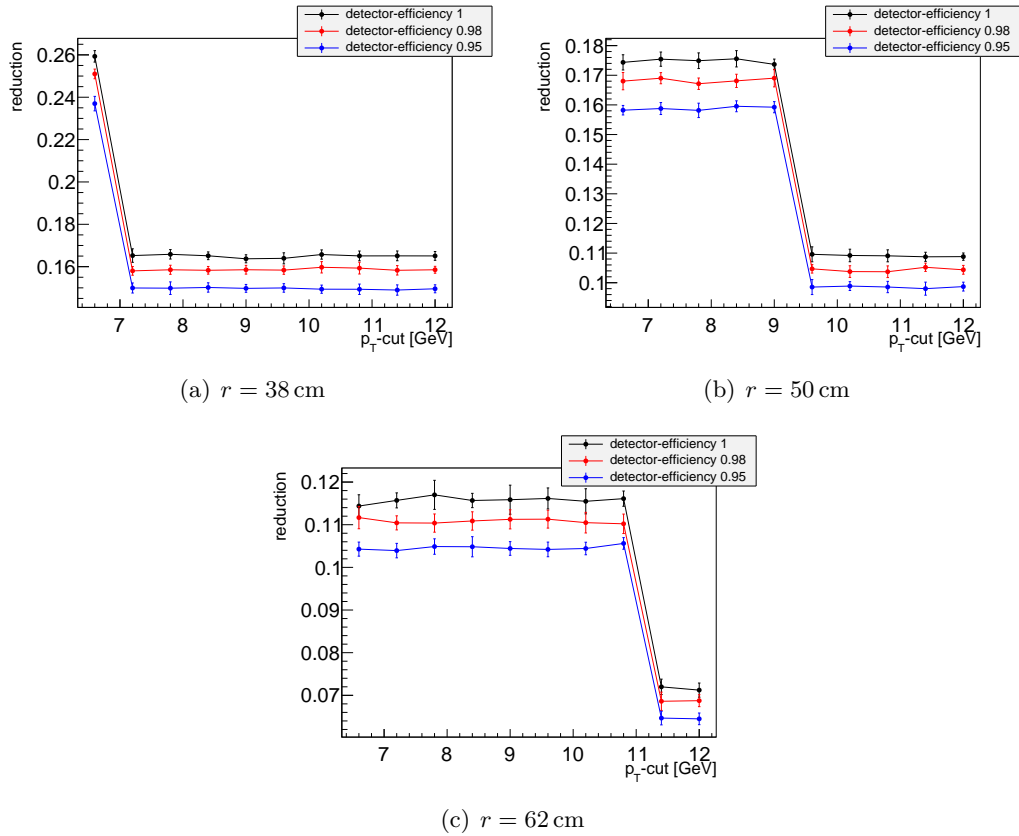


Figure 4.6.: Plot of the data reduction by the algorithm with respect to the underlying p_T cut for three different detector radii. The characteristic reduction step is the result of the offset resolution, which is determined by the double layer design. In this case shown is the step from the search interval $(\Delta n, \Delta z) \in [-2, 2] \times [-1, 1]$ to $(\Delta n, \Delta z) \in [-1, 1] \times [-1, 1]$.

This example also shows the high complexity of this problem. To implement it in hardware each strip has to be connected with the order of a thousand strips on the opposed layer. The only way to solve this problem is to reduce the maximum search offset, which is the subject of chapter 5.

4.3.2. Reduction of Data Volume

Also the data reduction plot of the combined algorithm shown in figure 4.6 differs only marginally from the one of the algorithm (cf. figure 4.2), which selects only complete coincidences with a small offset.

5. Cluster-Size-Method

The predominant problem of the hit assignments of the algorithms discussed in chapter 4 is the large number of interfering particles with a low transverse momentum. Another consequence of those low- p_T particles is shown in section 4.3.1. Particles with a low transverse momentum correspond to coincidences with very large offsets. Because of the likely possibility that two interactions with a large offset belong together, the reconstruction of lost interactions becomes impossible. Therefore the maximum search offset has to be reduced in order to implement an efficient reconstruction algorithm, which at the same time reduces the amount of data sufficiently.

One method to reduce the maximum search offset is to minimise and optimise it manually in a way that on hand the probability to reconstruct lost interactions increases and on the other hand not too many coincidences with a high offset form two isolated hits. Because of the large amount of particles with a low transverse momentum the latter instance leads to bad results for the data reduction. Therefore this method is not appropriate for the given objective of reducing the data volume.

Another method is to exploit an analogy between the double layer detector and its individual layers; similar to the offset a traversing particle induces on a double layer Δn , the distance between the entrance and exit point of the particle traversing a single layer $\delta(p_T)$ can be used to obtain information about the particle's transverse momentum. Because of the relatively small thickness of a few hundred μm of the silicon strip detectors, this distance is not very large.

The discretisation given by the 80 μm pitch in ϕ -direction for each strip only allows information about the number of joined strips, which are traversed by the particle. This number is referred to as cluster-size. Particles with a high cluster-size therefore can be considered of having a very low transverse momentum.

Filtering particles with a very low transverse momentum would not only lead to a decrease of occupancy and prevent low energetic particles from interfering but would also decline the maximum search offset.

This section concerns the quantification of the cluster-size and studies the possibility to utilise it in order to filter particles with a very low transverse momentum. The physics and geometry behind the cluster-size are similar to those of the offset of the double layer structure and can therefore be calculated by using equation 3.12. Hence the effects of varying parameters such as the thickness or the pitch of the silicon-strips can directly be studied.

5. Cluster-Size-Method

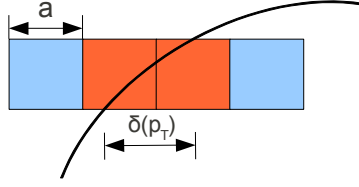


Figure 5.1.: Due to its low transversal momentum a traversing particle induces a hit in two joined silicon-strips. The distance between the entrance- and exit-point is referred to as $\delta(p_T)$.

In the last section of this chapter, the consequences of the decrease of the maximum search offset for the reconstruction algorithm presented in section 4.2 are presented.

5.1. Cluster-Size

The cluster-size states the number of joined silicon strips of a single layer, which are activated by the same traversing particle (cf. figure 5.1).

5.1.1. Filter Potential with respect to Silicon Thickness

One important parameter is the thickness of the used detector strips. The dependence between detector thickness and the cluster-size of particles with fixed transversal momenta can be calculated geometrically by equation 3.12. Figure 5.2 shows this relation for different transversal momenta.

ATLAS currently uses 250 μm thick silicon detector strips. As shown by figure 5.1 particles with a transverse momentum below 0.4 GeV would pass more than one strip detector in the actual idealised design. Hence, all particles having a transverse momentum below 0.4 GeV can be identified and filtered.

However, those interactions of particles with a low transverse momentum are not the only hits which would be filtered in reality. Even particles with a much higher transverse momentum than 0.4 GeV can pass more strips by traversing the single layer, which is illustrated in figure 5.3. Since the probability of a particle to enter the silicon-strip at position x is equally distributed among $[0 \mu\text{m}, 80 \mu\text{m}]$, the probability $P(p_T)$ that this particle induces a cluster-size greater than one, solely depends on its transversal momentum:

$$P(p_T) = \begin{cases} 1 & \forall \delta(p_T) > a \\ \frac{\delta(p_T)}{a} & \forall \delta(p_T) \leq a \end{cases} \quad (5.1)$$

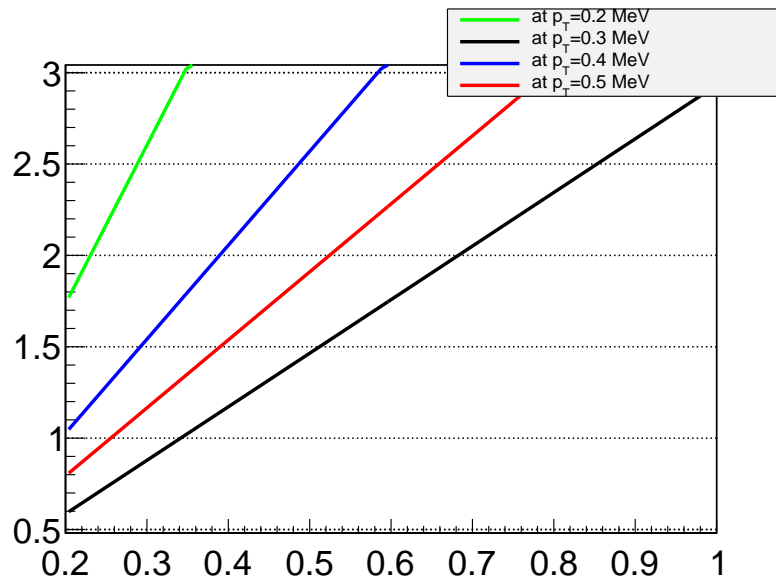


Figure 5.2.: Shown is the cluster-size with respect to the silicon-strip thickness at three fixed transversal momenta. At the actual strip design of 250 μm particles with a transversal momentum of 0.4 GeV have a cluster-size of approximately one.

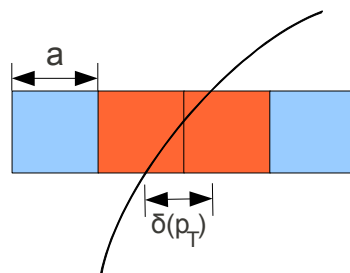


Figure 5.3.: A particle with a transversal momentum above 0.4 GeV passes two silicon strips. The distance between entrance point of the particle and the next silicon-strip is smaller than $\delta(p_T)$.

5.1.2. Reduction of Data Volume

Figure 5.4 shows the reduction of the data volume as result of filtering particles having a transverse momentum below a certain low- p_T cut. Because of the exponential increase of the number of particles, which are generated by the toy Monte Carlo, with respect to their p_T in the interval of [0.15 GeV, 0.75 GeV] (cf. 2.2.1) the shown plot is declines exponentially. At 0.4 GeV the overall data is reduced by 64 %.

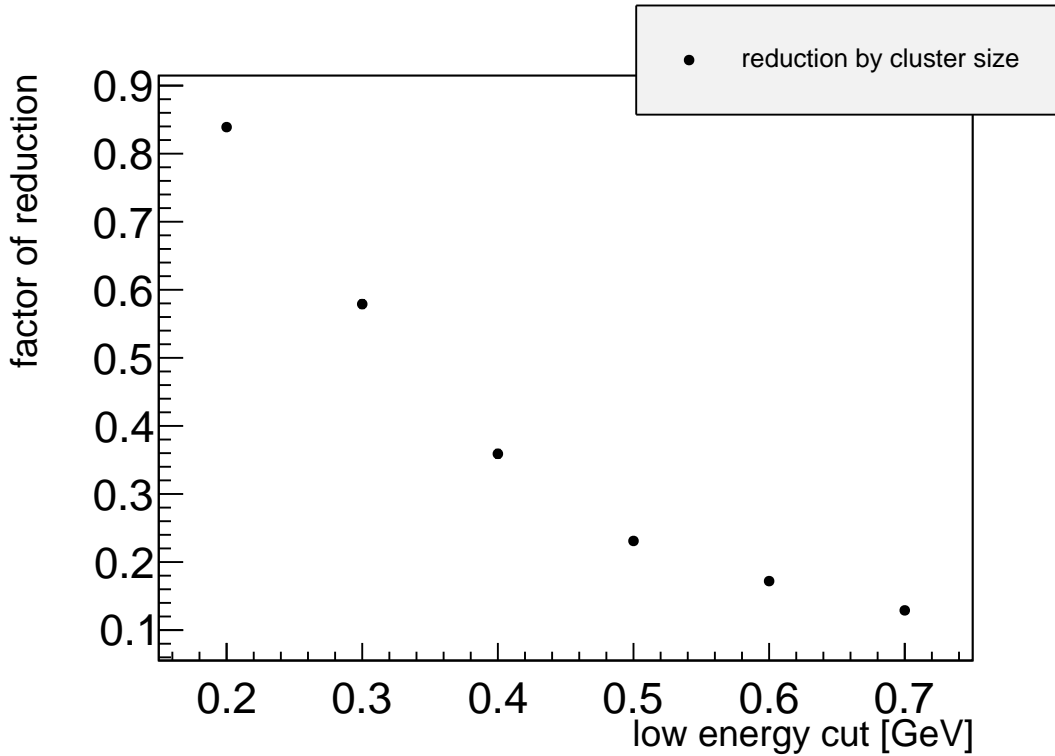


Figure 5.4.: Simulation of the reduction of the data volume with respect to a low- p_T -cut. All particles with a transverse momentum below this cut are filtered. At 0.4 GeV the overall data is reduced by 64 %.

The effect, that also particles with a high transverse momentum can have a cluster-size of two leads to more reduction potential than illustrated in figure 5.4, where the reduction of data due to an application of hard low energy cuts is shown.

Since the probability 5.1 that particles with a transverse momentum above the low- p_T -cut become filtered is similar for both layers, it will happen, that hits from the same particle have a cluster-size above one on the first layer and a cluster-size of one on the second layer and vice-versa. Therefore, simply ignoring all interactions with a cluster-size greater than one would lead to an additional single-hit inefficiency, which would have to be compensated by the reconstruction algorithm. Unfortunately the used toy

5.2. Efficiency Gain of the Combined Algorithm

radius [cm]	$p_{T_{min}}$ [GeV]	Δn_{max}	$\Delta n_{max}^{low-p_T-cut}$ (0.4 GeV)
38	0.11535	731	17
50	0.15135	839	23
62	0.18735	933	30

Table 5.1.: Shown are the minimum transverse momenta a particle has to have in order to reach the double layer detector for three different radii and the corresponding maximum search offsets. The last column shows the maximum search offset, corresponding to a low- p_T -cut of 0.4 GeV.

Monte Carlo does not provide any simulated information of actual cluster-sizes. Hence the present thesis uses only a hard low- p_T -cut at 0.4 GeV.

5.1.3. Decrease of the Maximum Search Offset

A low- p_T cut decreases the maximum search offset dramatically (cf. table 5.1).

5.2. Efficiency Gain of the Combined Algorithm

At an occupancy of 2 % on the inner most layer at $r = 38$ cm a hit on one of fifty strips is expected. Since the maximum search offset decreases to $\Delta n_{max} = 17$ the algorithm described in section 4.2 should now be able to reconstruct hits from high energetic particles.

By comparing figure 5.5 with figure 4.5 it becomes obvious that the algorithm is capable of reconstructing some lost interactions induced by particles with a high transverse momentum. Unfortunately the algorithm efficiency only increases to 94 % at 95 % single-hit-inefficiency of the detector. The reason, why the other 6 % are not found by the reconstruction algorithm is explained in chapter 6.

Figure 5.6 shows the factor of reduction obtained by the combined algorithm. The data reduction can be separated in two levels, which is demonstrated at the example of the inner most layer. In a first level the total amount of hits is reduced by approximately 64 % due to application of the cluster-size-method. In a second level the combined algorithm reduces the remaining 36 % to around 4 %.

5. Cluster-Size-Method

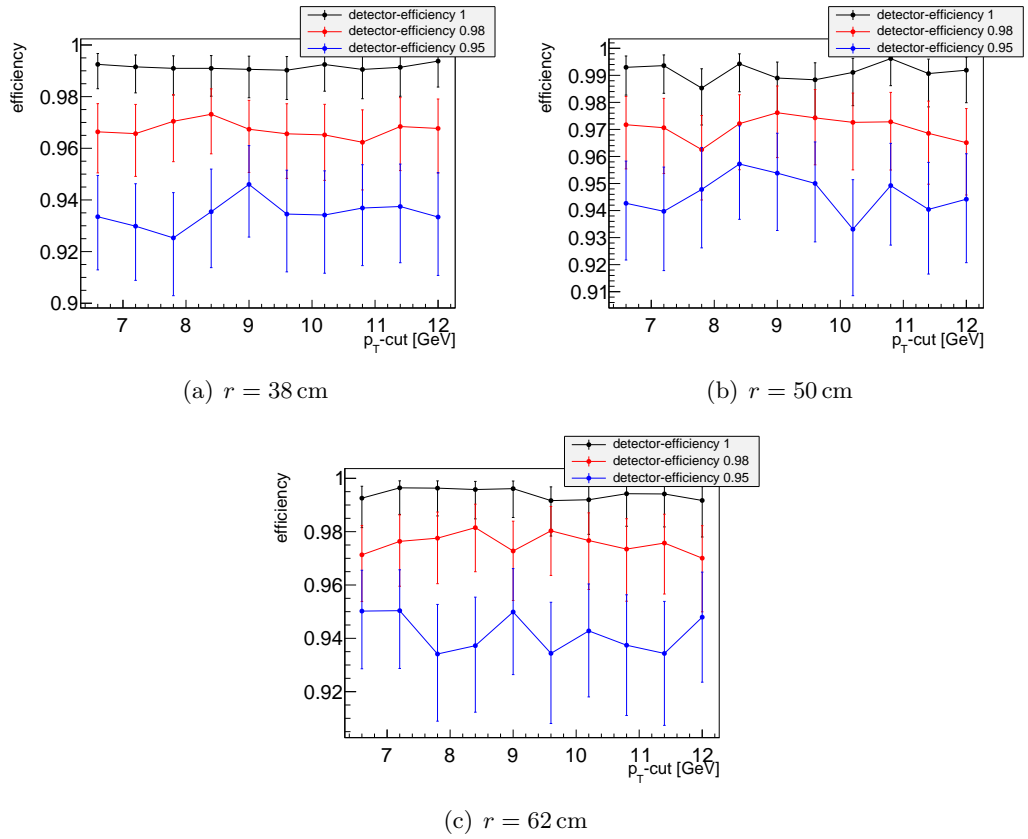


Figure 5.5.: Plot of the data reduction by the combined algorithm after applying the cluster size method for three different detector radii. Each plot shows the results of three simulations with different values of the single hit efficiencies of the detector.

5.2. Efficiency Gain of the Combined Algorithm

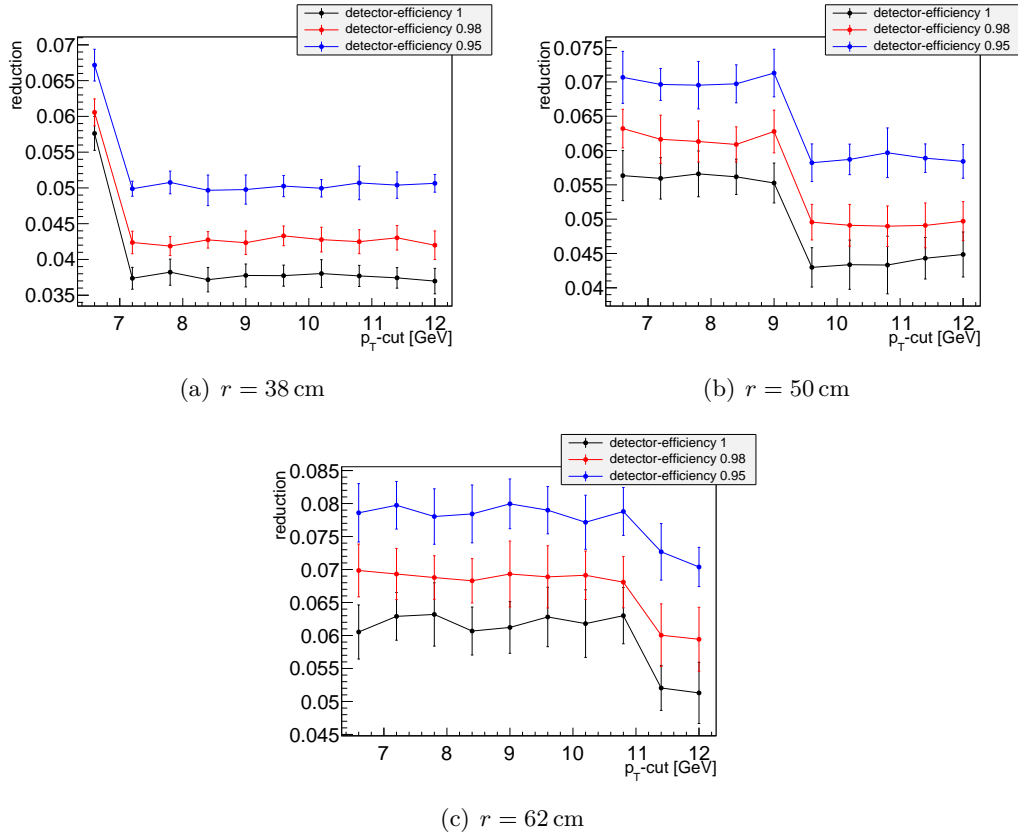


Figure 5.6.: Plot of the data reduction by the combined algorithm after applying the cluster size method for three different detector radii.

5. *Cluster-Size-Method*

6. Grouping Algorithm

Applying the cluster-size method to discard particles with a very low transverse momentum leads to better results for the combined algorithm (cf. section 4.2) from the perspective of the efficiency and the data reduction. As shown in figure 5.5 approximately 94 % of all particles having a transverse momentum above the highest resolvable p_T -cut are returned by the algorithm.

The first section of this chapter tries to explain why the other 6 % are not found, while the second chapter offers a solution for this problem.

6.1. Problem of the Combined Algorithm

Illustration 6.1 indicates why even after the application of the cluster-size method some lost interactions of high- p_T particles cannot be reconstructed by the combined algorithm. Even though there are no particles with a very low transverse momentum after applying the cluster-size-method, particles with a transverse momentum above 0.4 GeV mimic to be a possible associated hit of an interaction, whose real associated hit is lost.

In the example shown in illustration 6.1 the interaction between the high- p_T particle b and the outer detector layer is lost. Therefore the combined algorithm should reconstruct this interaction. Since the hit of the particle d on the outer layer is inside the maximum search region of the interaction of particle h , it is associated with the hit of particle h . Therefore the algorithm cannot identify the interaction of the h -particle on

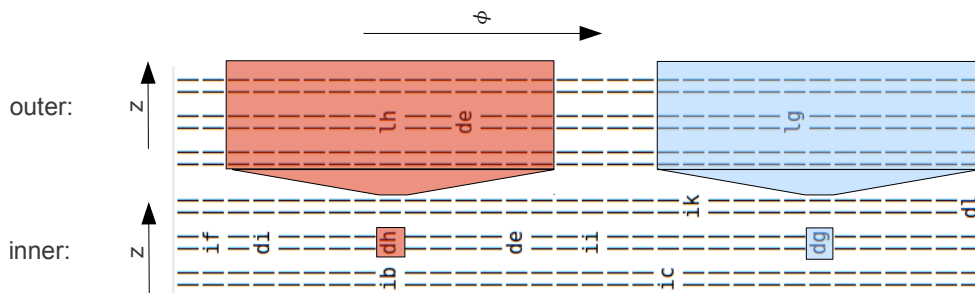


Figure 6.1.: Illustration of the main reason, why the combined algorithm cannot reconstruct all lost interactions.

6. Grouping Algorithm

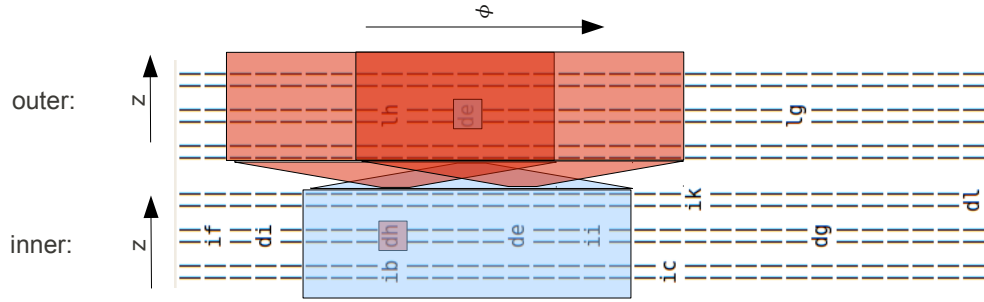


Figure 6.2.: Illustration the modus operandi of an algorithm, which forms small and isolated groups of hits.

the inner layer as isolated hit (red). In fact the algorithm filters this interaction, since the algorithm assumes it to be induced by a particle, whose transverse momentum is not high enough to be considered as interesting. Particle d is correctly considered as lost hit (blue), since no interaction is inside its maximum search region on the opposed layer. Therefore it forms a group with one hit.

Obviously even interactions of particles which induce a coincidence with a relatively small offset sometimes mimic to be a possible associated hit of a hit, whose real associate is lost.

6.2. Problem Solving

The main idea to reconstruct even those particles is to exploit the low occupancy, the absence of particles with a very low transverse momentum and the small maximum search offset provided by the cluster-size-method to form small isolated groups of hits. These groups are called isolated, because all possible associated hits of each group member belongs to its group. Hence no interaction between different groups is needed in order to associate hits correctly. Because of the low occupancy it is highly unlikely that hits of many different particles interfere in the maximum search region of each other. Therefore the average number of interactions per group has to be small.

Figure 6.2 tries to visualise the idea on the same example, which was used to describe the problem.

The algorithm starts at the interaction between particle h and the inner detector layer (pink) and scans the opposed layer for hits inside the maximum search region (red left). Thereby it finds the interaction de . Since all possible associated hits of each group member should also be in the group, the algorithm has to search for all hits, which could possibly be associated with the e -interaction on the outer layer. Hence the algorithm scans the maximum search region on the inner layer (blue) and finds the interaction induced by particle e . In a last step the maximum search region of the

interaction de is scanned (red right). Since the interaction de already belongs to the group no further scanning is necessary. The group forming is finished.

In the next step for each group the number of hits on the inner layer is compared to the number of hits on the outer layer. If they are not equal, the algorithm considers all interactions on the layer with the greater number of hits to be a part of a coincidence, whose second hit is lost. Hence all interactions are returned as possible trigger candidates.

6.3. Implementation of Grouping

Since for each coincidence an additional offset in z -direction also has to be taken into account forming groups the way described in section 6.2 becomes much more complex. However, one has to allow groups to be two dimensional, because otherwise 24 % of all groups would be considered to have a member, whose associated hit is lost. Hence the reduction of data would decrease.

Another reason because an algorithm with low complexity is needed, is that it has to be implemented in hardware.

Therefore in the following an implementation is described, which tries to fulfil those constraints on complexity as good as possible. Figure 6.3 shows an extract of a hit pattern before grouping. This illustration can be used to comprehend the algorithm described in the following.

The first step is to make each hit on the double layer to its own group. Afterwards for each hit on the inner layer the algorithm searches for all interactions on the opposed layer, which potentially originate from the same particle, i. e. are inside the maximum search region of each other. If a hit on the outer layer is found, then both the group of the found interaction and the group of the primary interaction will become congregated.

Figure 6.4 shows an extract of a hit pattern on which the grouping algorithm was applied.

6.4. Efficiency

Figure 6.5 shows the efficiency of the algorithm presented above. Even at a single hit detector inefficiency of 5 % this algorithm relays above 98 % of all high energetic particles.

Although this algorithm emerges as highly efficient (cf. figure 6.5), there are still some cases left in which it cannot recover lost high energetic particles; if, for instance, on both layers a hit gets lost, which do not originate from the same particle, then

6. Grouping Algorithm

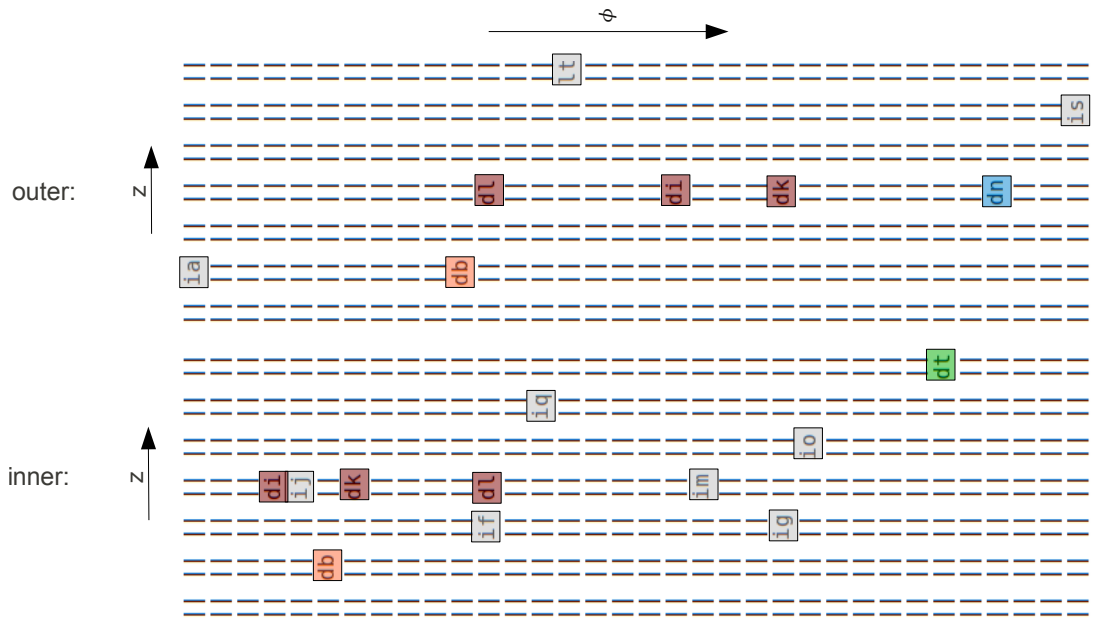


Figure 6.3.: Shown is the region $(\Delta n, \Delta z) \in [-17, 17] \times [-3, 3]$ of the double layer detector at $r = 38$ cm, containing four clusters (red, orange, green and blue) as well as several particles, which are either ignored or lost (grey).

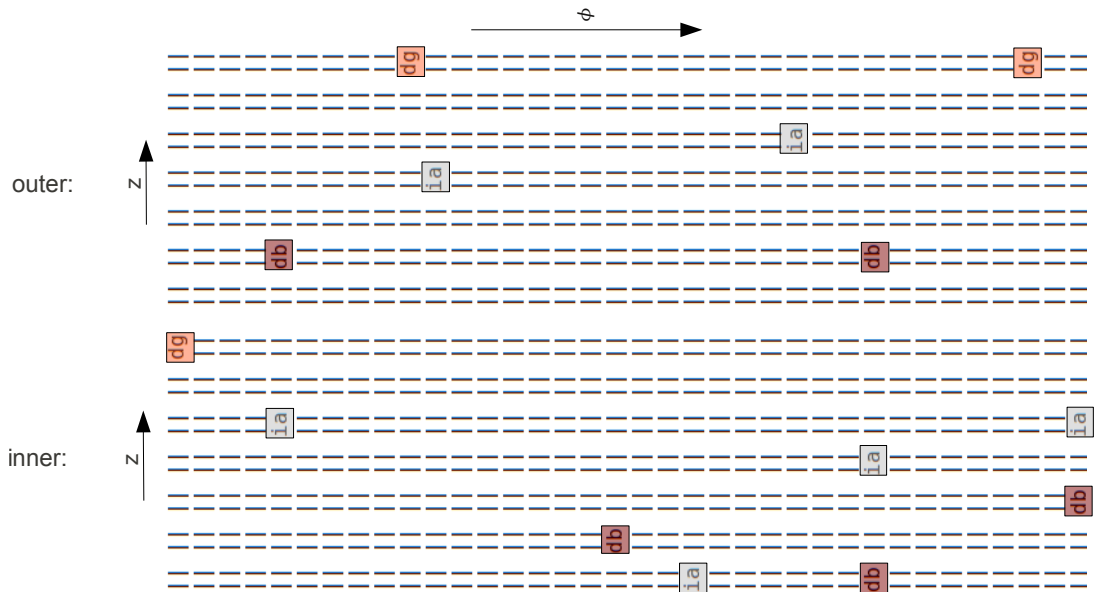


Figure 6.4.: Shown is the region $(\Delta n, \Delta z) \in [-17, 17] \times [-3, 3]$ of the double layer detector at $r = 38$ cm after grouping. The second character does not state the particle ID, but instead the cluster ID.

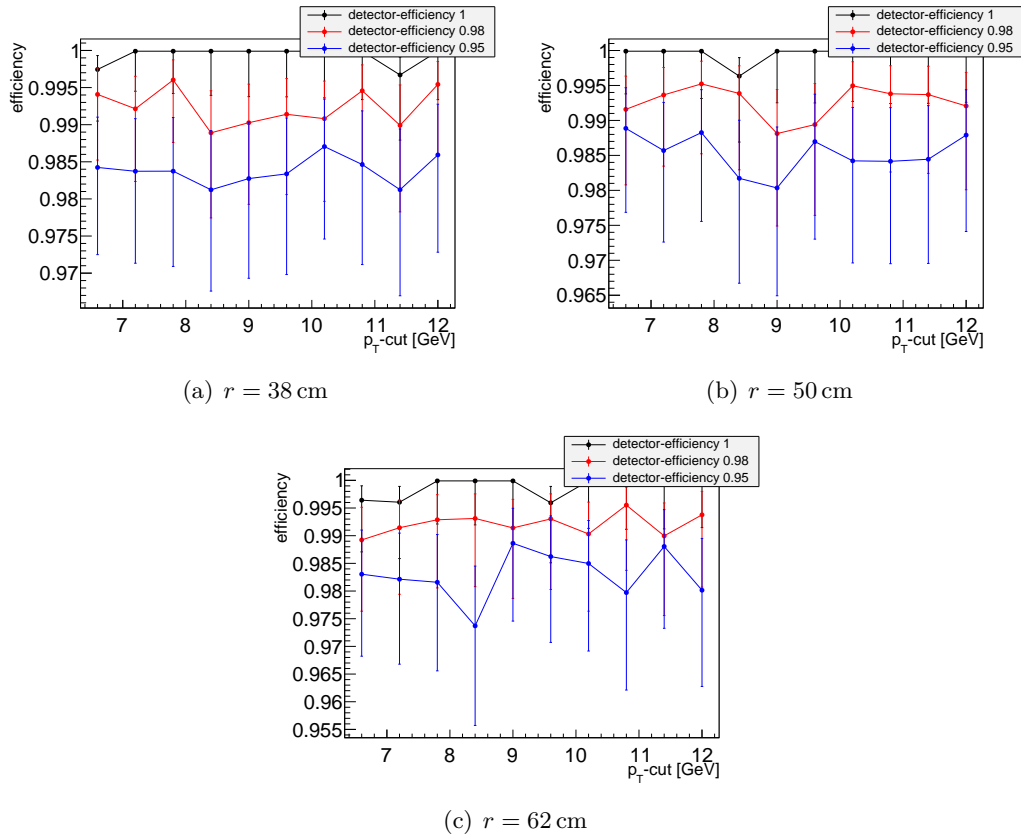


Figure 6.5.: Plot of the algorithm efficiency with respect to the underlying p_T cut for three different detector radii. Each plot shows the results of three simulations with distinct single hit efficiencies of the detector.

6. Grouping Algorithm

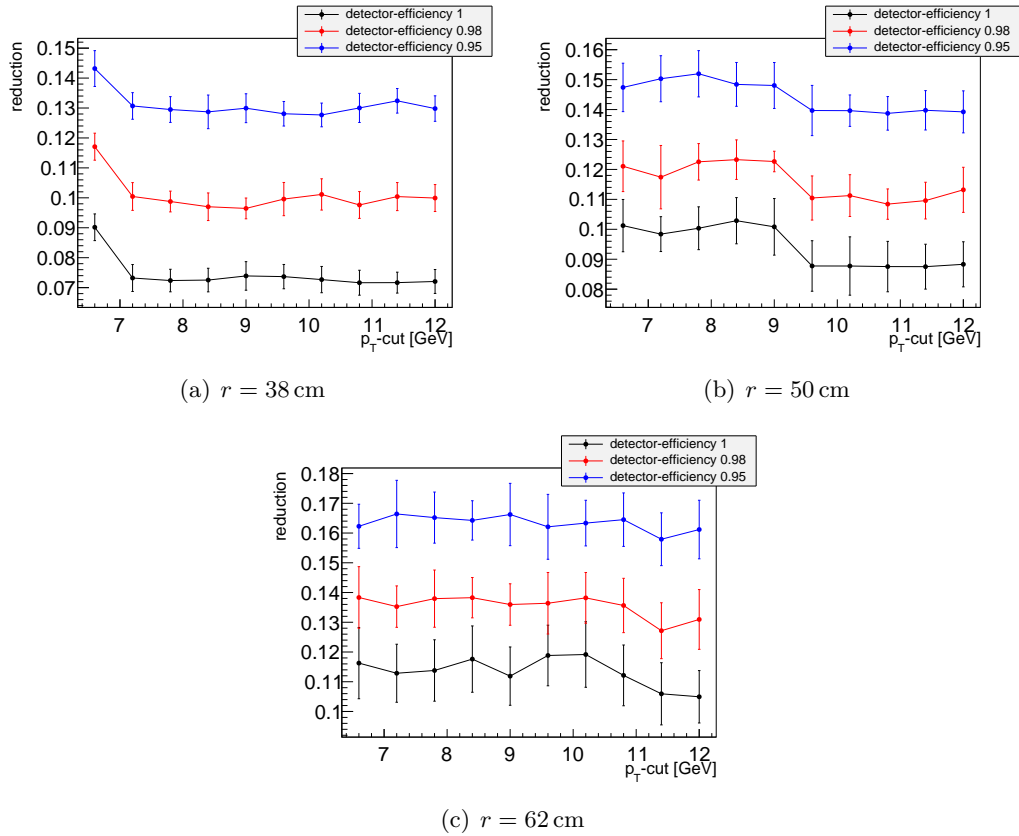


Figure 6.6.: Plot of the data reduction by the algorithm with respect to the underlying p_T cut for three different detector radii.

the number of hits on the inner layer is equal to the number of hits on the outer layer. Hence the algorithm does not relay any of those interactions as possible trigger candidates.

6.5. Reduction of Data Volume

Because of returning all interactions of the layer, which has more interactions than the other, for each group, even more than all coincidences with a lost interaction ($\simeq 1 - \epsilon_{det}^2$ % of all data) are returned as candidates for interactions induced by a high- p_T particle. Figure 6.6, which shows the overall reduction of the data volume for different detector-barrel radii and single-hit-inefficiencies, supports those considerations.

At a detector-efficiency of 0.95 % all plots show that the over all reduction, i. e. the reduction obtained by using the cluster-size-method and the algorithm, is approximately 85 %.

7. Conclusion

Several methods and algorithms to exploit the double layer structure of the SCT barrels in order to reduce the bandwidth and compensate single-hit-inefficiencies of the strip detector in a first trigger level, have been studied. Within those studies the necessity of an additional approach to discard particles with a very low transverse momentum became obvious. Hence the cluster-size-method was presented. Since the used toy Monte Carlo does not provide any information about the cluster-size, it was simulated by the application of a hard high- p_T -cut at 0.4 GeV. In a last step an algorithm was introduced, which uses the advantages provided by the cluster-size-method in order to reconstruct as many high- p_T -particles as possible under the constraint to keep the reduction of bandwidth as low as possible.

In the following sections the results of the different algorithms from the perspective of efficiency and data reduction are summarised at the example of the inner most detector barrel at $r = 38$ cm.

7.1. Algorithm Efficiency

Figure 7.1 shows the efficiency graphs for all presented algorithms at a single-hit-inefficiency of the detector-strips of 95 %. Because of the large number of particles having a very low transverse momentum and therefore form coincidences with a high offset the first approach to reconstruct lost interactions did not work. Its efficiency is located around the expected efficiency of an algorithm without reconstruction methods (90.25 %).

However, after applying the cluster-size-method the same reconstruction algorithm reached an efficiency of 94 %.

The most efficient algorithm is the grouping algorithm, since it finds almost all lost hits, which reduces its performance in data reduction. It returns above 98 % of all particles having a transverse momentum above a given high- p_T -cut.

7.2. Reduction of Data Volume

Similarly to the efficiency graphs figure 7.2 shows the reduction graphs for each algorithm at a single-hit-inefficiency of 95 %.

7. Conclusion

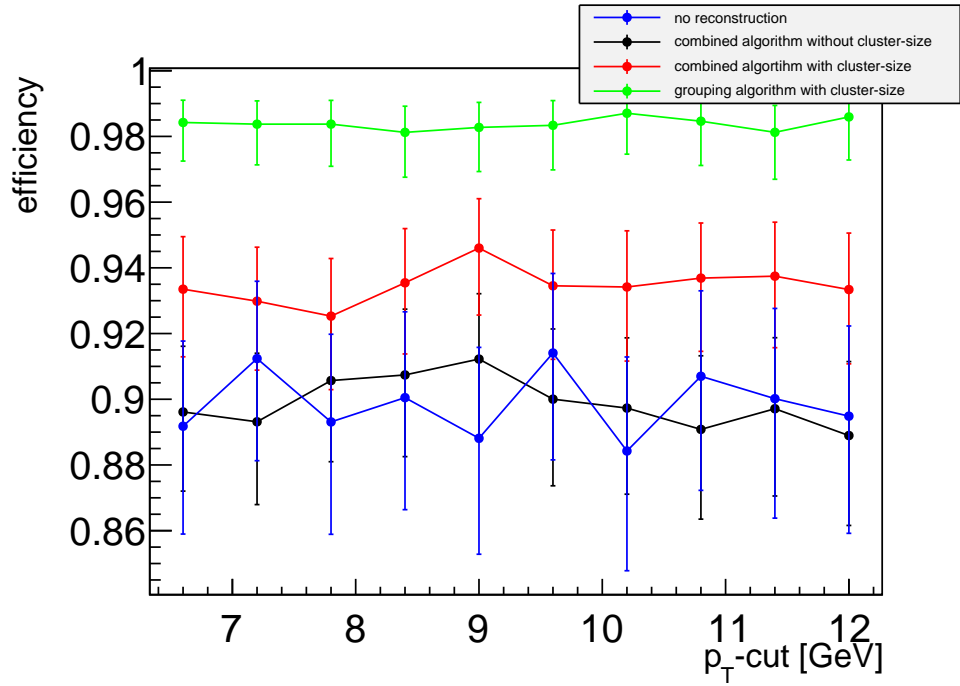


Figure 7.1.: Plot of the algorithm efficiency with respect to the underlying p_T cut for three reconstruction algorithms, which are compared to an algorithm without reconstruction. Each plot shows the results for the inner most detector-barrel at a single-hit-inefficiency of 0.95 %.

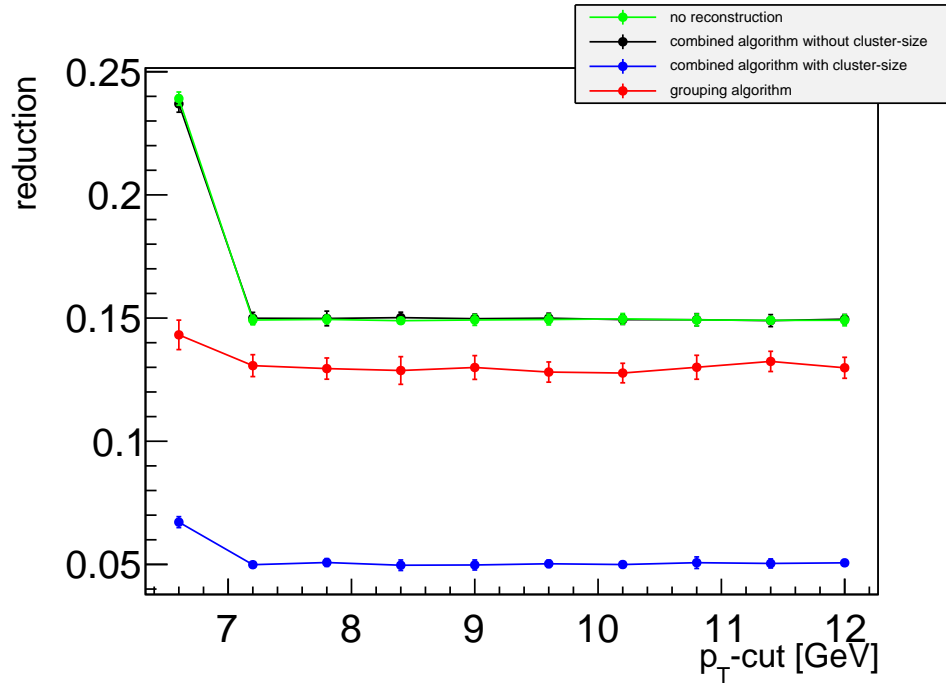


Figure 7.2.: Plot of the algorithm efficiency with respect to the underlying p_T cut for three different detector radii. Each plot shows the results of three simulations with distinct single hit efficiencies of the detector.

Obviously the combined algorithm has the best performance in data reduction. It returns only 5 % of all data, which contains approximately 94 % of all high- p_T tracks.

The grouping algorithm on the other hand reduces the data only by a factor of 85 %. Therefore it recovers almost every high- p_T track. The optimisation of this correlation was the key-note of the present thesis.

7. Conclusion

A. Definitions and Illustrations

A.1. Hit

A detected interaction between a silicon strip and a particle is called *hit*.

A.2. Coincidence and Offset

Typically one traversing particle causes a hit on the inner and outer layer. Both hits form a *coincidence* with a certain offset Δn in ϕ -direction depending on the transverse momentum p_T of the particle.

A.3. Hypothetical Coincidences

All of the algorithms used in this thesis matches a hit on the inner and on the outer layer and therefore assume coincidences, which are called *hypothetical coincidences*. Some of this hypothesis will turn out to be correct (*correct coincidence*) and some will not (*fake coincidence*).

A.4. Lost Hits

Due to inefficiencies of the detector sometimes a hit on the inner or on the outer layer is not detected. This event will be referred to as *lost hit* - its remaining affiliate will be called *lonely hit*.

In order to compensate lost hits the algorithms should be able to generate hits in certain cases. Those assumed hits will be called *virtual hits* since they were not detected in reality. Additionally the algorithms will assume a coincidence between the lonely and the virtual hit.



Figure A.1.: Detected interaction between silicon strip and particle in green.

A. Definitions and Illustrations

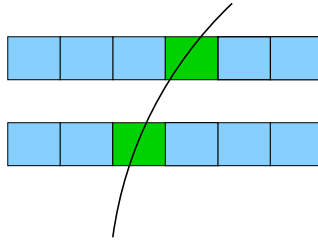


Figure A.2.: Coincidence with offset $\Delta n = 1$ in green.

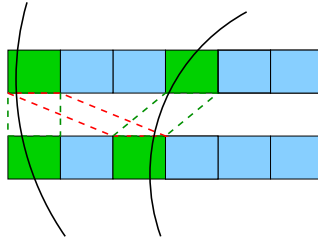


Figure A.3.: Shown are hypothetical coincidences (dashed lines). Some of them are correctly assigned (green) and some not (red).

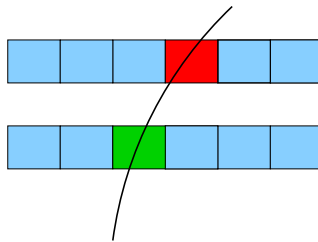


Figure A.4.: Shown is the lost hit in red and the lonely hit in green.

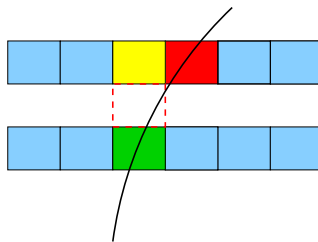


Figure A.5.: Due to inefficiency the interaction on the outer layer gets lost (red). Since the hit on the inner layer becomes a lonely hit (green) in this example the algorithm assumes the vis-à-vis strip to be inefficient and therefore generates a virtual hit (yellow) and connects both by an assumed coincidence, which in this case is false.

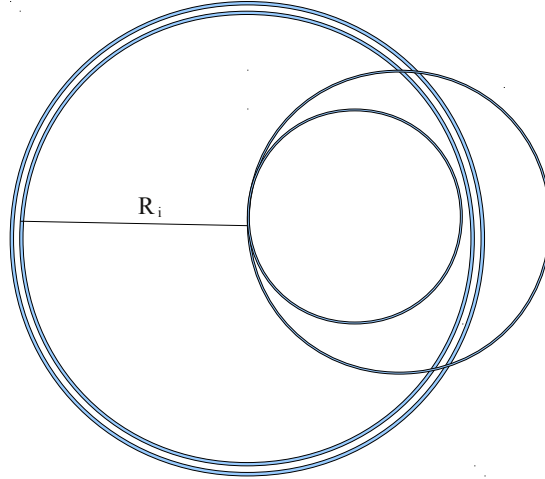


Figure A.6.: Illustration of equation A.1. Shown are two particles with different p_T . The particle on the inner circle does not reach the SCT-layer due to its low transversal momentum.

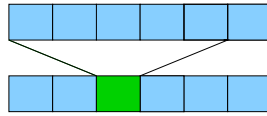


Figure A.7.: Shown is the area around a hit on the inner layer defined by $\Delta n_{max} = 2$

A.5. Maximum Search Offset

One important parameter used by all algorithms is the *maximum search offset* Δn_{max} . It defines the region on the opposed layer where the algorithm is allowed to find associated hits. Generally this parameter is given by the parameters of the experimental setup since there is a minimal transverse momentum $p_{T_{min}}$ - and therefore a maximal offset Δn_{max} - particles must have to be able to reach the detector (cf. figure A.6). This transverse momentum can be calculated as follows:

$$R_i + d \stackrel{!}{=} 2r = \frac{2p_{T_{min}}}{cqB} \Leftrightarrow p_{T_{min}} = \frac{cqB(R_i + d)}{2} \quad (\text{A.1})$$

Using equation 3.12 with p_{min} leads to the maximum search offset Δn_{max} . However, this parameter can be adjusted, which may become necessary for a high occupancy. Note that the maximum search offset is an absolute integer value, because positive and negative ϕ -direction will be treated equally.

A. Definitions and Illustrations

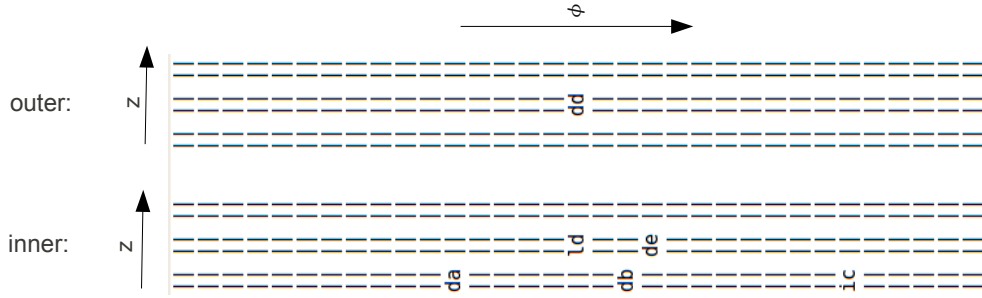


Figure A.8.: Shown is an excerpt of the innermost SCT-barrel in the format $(|\Delta n|, |\Delta z|), \epsilon [0, 15] \times [0, 1]$. Particle d only induced a hit on the outer layer. The corresponding hit on the inner layer got lost.

A.6. Reduction of Data

The reduction of data will be indicated as the ratio of particles being considered as high energetic candidates and the overall number of particles which have reached the inner layer.

A.7. Algorithm Efficiency

The number of high energetic particles, which were actually found by the algorithm divided by the number of high energetic particles which have reached the inner layer will be referred to as the algorithm efficiency.

A.8. Detector Efficiency

The detector efficiency is the probability that an interaction between detector-strip and particle is detected.

A.9. Illustrations of Simulated Hit Pattern

The Algorithms will also be introduced graphically. In order to represent them as accurate as possible simulated hit pattern will be used to illustrate their functionality and problems, which may occur. Figure A.8 shows an accordant illustration.

Both detector layers are represented by three lines. An interaction between a particle and a detector strip is encoded with two characters. The first states the status of the particle; d stands for a **d**etected interaction, l indicates an interaction which has

A.9. Illustrations of Simulated Hit Pattern

gone lost due to a detector inefficiency and i states particles which are determined as low-energetic and therefore will be ignored by the algorithm. The second character identifies the particle, which caused the interaction.

In the example shown in figure A.8 the particle d traversed the observed double-layer excerpt. Only a hit on the outer layer was detected by the detector. The interaction on the inner layer has gone lost and thereby will not be taken into account by any of the algorithms.

A. Definitions and Illustrations

Bibliography

- [1] The ATLAS Collaboration, G Aad et al, “The ATLAS Experiment at the CERN Large Hadron Collider,” *JINST*, vol. 3, no. S08003, 2008.
- [2] Michelangelo L. Mangano, “The super-LHC,” *arXiv.org:0910.0030*, 2009.
- [3] F. Englert and R. Brout, “Broken Symmetry and the Mass of Gauge Vector Mesons,” *Physical Review Letters*, vol. 13, pp. 321 – 332, 1964.
- [4] P. Higgs, “Broken Symmetries and the Masses of Gauge Bosons,” *Physical Review Letters*, vol. 13, pp. 508 – 509, 1964.
- [5] C. Amsler et al., “Review of Particle Physics,” *Physical Letters B*, vol. 667, 2008.
- [6] A. Abdesselam, “High Luminosity Upgrade.” <http://atlas.web.cern.ch/Atlas/GROUPS/UPGRADES/>, accessed in June 2010.
- [7] L. Evans and P. Bryant, “LHC Machine,” *JINST*, vol. 3, no. S08001, 2008.
- [8] J. Tseng, “ATLAS Upgrade Plans for the SLHC,” *Nuclear Physics B*, vol. 177-178, pp. 212–216, 2008.
- [9] S. Agostinelli et al., “Geant4 - a simulation toolkit,” *Nuclear Instruments and Methods in Physics Research Section A*, vol. 506, 2003.
- [10] Daniel Glodeck, “Simulation eines L1-Spur-Triggers für ATLAS.” Bachelor Thesis.
- [11] N. Konstantinidis, “ATLAS L1 track trigger for super-LHC,” *Proceedings of Science*, 2010.
- [12] H. Bethe, “Zur Theorie des Durchgangs schneller Korpuskularstrahlen durch Materie,” *Annalen der Physik*, vol. 397, 1930.
- [13] ATLAS Collaboration, “Charged-particle multiplicities in pp interactions at $\sqrt{s} = 900$ GeV measured with the ATLAS detector at the LHC,” *Phys. Lett. B*, vol. 688, pp. 21–42, 2010.

Erklärung

Ich versichere, dass ich diese Arbeit selbstständig verfasst und keine anderen als die angegebenen Quellen und Hilfsmittel benutzt habe.

Heidelberg, den 25. Juli 2010

Unterschrift: _____